

# Finite Temperature Effects in the Nonintegrable $SU(3)$ Lipkin Model

M. O. Terra<sup>\*,†</sup>

*Instituto de Física, Departamento de Física-Matemática, Universidade de São Paulo,  
C.P. 66318, 05315-970 São Paulo, SP, Brazil*

M. C. Nemes<sup>‡</sup>

*Departamento de Física, ICEX, Universidade Federal de Minas Gerais,  
C.P. 702, 30161-970 Belo Horizonte, MG, Brazil*

and

C. da Providência and J. da Providência

*Centro de Física Teórica, Departamento de Física, Universidade de Coimbra,  
P-3000 Coimbra, Portugal*

Received December 5, 1996; revised May 5, 1997

In the present work we use nonrelativistic many body physics techniques to generalize the classical limit of quantum systems in such a way as to incorporate statistical mixtures. Finite temperature effects are thus incorporated in a natural way. We give a detailed account of the thermodynamics of the  $SU(3)$  Lipkin model and then derive the classical thermal (chaotic) dynamics of the system. The most remarkable features of our analysis are twofold: firstly the appearance of a new degree of freedom essentially connected to thermal effects, i.e., for high enough temperatures. Secondly we give a quantitative characterization of the temperature effects on the chaotic volume of the system. Thermal effects are shown to be responsible for novel nonlinear contributions to the dynamics and to consistently counterbalance the interaction part of the dynamics. This is the case in the context both of thermodynamics and of the thermal dynamics and we believe it to be true in general. © 1998 Academic Press

## I. INTRODUCTION

The discovery of chaotic phenomena with manifestly universal characteristics in so many different areas of science can undoubtedly be considered as one of the

\* Present address: Instituto de Física, Departamento de Física do Estado Sólido e Ciência dos Materiais, Universidade Estadual de Campinas (UNICAMP), C.P. 6165, 13083-970, Campinas, SP, Brazil.

† E-mail address: maisa@ifi.unicamp.br.

‡ E-mail address: carolina@cedro.fisica.ufmg.br.

most fascinating challenges of this century. In particular Mathematics and Physics have largely contributed to unveiling the origins and consequences of such general and interdisciplinary phenomenon. In this context a most remarkable achievement in what concerns the understanding the structural manifestations of chaos is the KAM theorem [1], proposed and proved originally by Kolmogorov in 1954 and later revised and proved in detail by Arnold (1963) and Moser (1962). On the other hand a lot of our present knowledge of the phenomenon is due to the impressive technological development in computer sciences which allowed for the numerical studies of non linear problems and the detailed investigation of specific models.

Chaotic behavior has been subject of intense investigation in physics. The two main branches of investigation are chaos in dissipative systems [2, 3] and hamiltonian chaos [4–6]. The present work belongs to the latter. We aim at an extension of the idea of the classical limit as traditionally understood, as a variational independent particle approximation. Independent particle states are the so called generalized coherent states [7–10]. A natural extension consists in the use of independent particle statistical mixtures as the set of variational density matrices and allows for the study of finite temperature effects on classically chaotic systems, which remains yet relatively unexplored. The previously obtained results by the present authors are restricted to Dicke’s maser model [11, 12] for which, due to its too simple mathematical structure, the thermal effects on the chaotic dynamics are rather trivial. They amount to a scaling in the allowed phase space. In this case, therefore the thermal dynamics can be completely mapped on the zero temperature dynamics.

The classical limit of Lie algebras, including  $SU(3)$ , not in the context of coherent states has recently been studied by different authors [13, 14]. In particular a specific realization of the  $SU(3)$  algebra was given in [13] and a general prescription for the definition of the classical dynamics of any Lie algebra in terms of Poisson brackets, independent of the representation, was discussed in [14]. Using the Lie–Poisson approach of ref. [14] and the method proposed in ref. [15, 16] in order to include the effects of a heat bath, the thermodynamic properties of systems described by algebraic Hamiltonians have been studied in [17].

In the present work, the variational states that lead to the extended classical dynamics are chosen to be a set of mixed states which are unitarily equivalent to the thermodynamical equilibrium state [18, 19]. Thus, the resulting dynamics will be hamiltonian and through the variational states, temperature dependent. For this reason the important first step consists in studying in detail the thermodynamics of the model under question. We have implemented the discussed technique within the context of an  $SU(3)$  version of the Lipkin–Meshkov–Glick<sup>1</sup> model [20, 21]. This model was proposed originally to test many-body techniques and more recently it has been revisited in the context of “quantum chaos”, semiclassical limit [22–27] and the theory of large amplitude collective motion [28].

The two main reasons which lead to the choice of this model were: firstly its mathematical structure is extremely rich and therefore contains, as we will show,

<sup>1</sup> For simplicity from now on this model will be referred to as *the LMG model*.

highly nontrivial thermal effects such as the appearance of a new degree of freedom. We investigate in detail the competition between dynamical effects coming from coupling terms in the Hamiltonian and temperature effects. Secondly there is the fact that the Lipkin model belongs to a class of exactly soluble models, Curie-Weiss models [29] which possess the interesting property that the mean field approximation becomes exact when the expansion parameter (in this case the number of particles of the system) tends to infinity [30, 31]. In other words the LMG model has a mathematically well defined classical limit.

Several finite temperature approaches to the study of the properties and phase transitions of the LMG model and other group theoretical Hamiltonians have been performed including thermal boson mappings [32], finite-temperature Hartree-Fock [33], corrections to the finite temperature mean field such as the static path approximation [34] and the correlated finite temperature Hartree-Fock [35].

The thermodynamics of the model reveals two second order phase transitions and therefore three distinct regimes which we call *Strong Coupling Regime* (SCR), *Intermediate Coupling Regime* (ICR) and *Weak Coupling Regime* (WCR). In the SCR the interaction part of the Hamiltonian plays a dominant role in determining the thermodynamic properties. As temperature increases, the system goes over to the ICR where the dynamical effects are partially neutralized by the thermal effects. Finally, for high enough temperatures the phase transition to the WCR takes place and the system is completely governed by thermal effects. This behavior is reflected in the average values of the Casimir operators of the group in question: for low temperatures, the SCR can be thought of as being completely characterized by the symmetric representation of the group. As temperature increases, close to the phase transition, other representations start to contribute.

The study of the thermal dynamics is a very complex task, as opposed to the integrable  $SU(2)$  version of the model, where thermal effects again amount to a phase space scaling [36, 37]. The number of the fixed points in the  $SU(3)$  dynamics is now fourteen (compared to four in the integrable case [24]). We have studied the behavior of the fixed points as a function of the temperature for the SCR regime.

We have also analysed the interplay between chaos and temperature: in the SCR we find a scaling behavior and the thermal chaotic dynamics can be mapped onto the zero temperature one. This trivial scaling behavior disappears, however, as the temperature increases. In particular we show the appearance of a new (third) degree of freedom which is essentially connected to thermal effects. In this case, although Darboux theorem [1] guarantees the existence of pairs of canonically conjugate variables, we have been unable to construct them by a useful method for practical purposes, in spite of all our efforts. Fortunately this is not necessary to give a quantitative characterization of the chaotic volume of the system. We have in these cases (ICR, WCR) directly integrated Heisenberg's equations of motion for the average values of the generators of the algebra, thus determining the Lyapunov's exponents and defining the chaotic volume. According to this criterion we have shown that the chaotic volume decreases as a function of temperature.

The present work is organized as follows: in Section II we briefly sketch the variational method used. Section III contains a definition of the  $SU(3)$  Lipkin model. Its thermodynamical properties are contained in Section IV and the thermal dynamics in Section V. Conclusions can be found in Section VI.

## II. MEAN FIELD APPROXIMATION FOR MIXED STATES

Let  $H$  be the Hamiltonian for a  $N$  particles system. An arbitrary mixed state of this system is described by a density matrix  $D$  such that

$$\text{Tr}(D) = 1. \quad (1)$$

The time evolution of  $D$  is governed by Liouville–von-Neumann equation

$$\dot{D} = i[D, H], \quad (2)$$

or equivalently

$$D(t) = e^{-iHt} D(0) e^{iHt}. \quad (3)$$

A stationary state  $D_0$  satisfies

$$[H, D_0] = 0. \quad (4)$$

The above condition can be formulated variationally. For this purpose we consider a set of unitarily equivalent trial density matrices

$$D(t) = \mathcal{U}(t) D_0 \mathcal{U}^\dagger(t), \quad (5)$$

where  $\mathcal{U}(t)$  is an arbitrary unitary operator which is labelled by variational parameters. The resulting dynamics will be hamiltonian.

Technically it is much simpler to work with the diagonal form of  $D_0$ ,

$$D_{dg} = V D_0 V^\dagger, \quad (6)$$

where  $D_{dg}$  is a diagonal time independent density and  $V$  the adequate (also time independent) unitary transformation. We can thus rewrite (5) as

$$D(t) = U(t) D_{dg} U^\dagger(t), \quad (7)$$

provided  $U(t) = \mathcal{U}(t) V^\dagger$ .

The mean field approximation consists in choosing  $D_{dg}$  and  $U(t)$  such that

$$D_{dg} = \exp(A)/\text{Tr}(\exp(A)) \quad \text{and} \quad U(t) = \exp(iS(t)), \quad (8)$$

where  $A$  and  $S$  are Hermitian one body operators and the most general form of  $U(t)$  is parametrized by a set of complex variables  $\{\alpha_1, \alpha_2, \dots, \alpha_n\}$ .

Statistical equilibrium is obtained by minimizing the free energy of the system, i.e.,

$$F = \text{Tr}(DH) + \frac{1}{\beta} \text{Tr}(D \ln D), \quad (9)$$

where  $\beta = 1/k_B T$ . Here,  $k_B$  is the Boltzmann's constant and  $T$  stands for temperature. The first term on the r.h.s. is the internal energy and the last one the system's entropy  $S = -k_B \text{Tr}(D \ln D)$ .

The dynamical equations of motion for the set of the parameters  $\{\alpha_1, \alpha_2, \dots, \alpha_n\}$  are obtained by minimizing the action

$$I = \int_{t_1}^{t_2} L dt, \quad (10)$$

where

$$L = i \text{Tr}(D_{dg} U \dot{U}^\dagger) - \text{Tr}(D_{dg} U H U^\dagger). \quad (11)$$

It is well known that this Lagrangian is variationally equivalent to the Liouville–von Neumann equation for the time evolution of the density matrix, Eq. (2). We sketch the proof of this fact. At any time  $t$  the density matrix  $D(t)$  can be written in terms of the stationary density matrix  $D_0$ , as

$$D(t) = U^\dagger(t) D_{dg} U(t), \quad (12)$$

where  $U(t)$  is a unitary operator. We denote by  $\delta F$  an infinitesimal hermitean time-dependent one-body operator satisfying

$$\delta U = -i U \delta F, \quad \delta U^\dagger = i \delta F U^\dagger.$$

We require that  $\delta I$  does not depend on  $\delta F(t)$ , for  $t_1 < t < t_2$ . Then, simple algebra shows that

$$\int_{t_1}^{t_2} dt \text{Tr}(\dot{D} - i[D, H]) \delta F = 0. \quad (13)$$

Since  $\delta F$  is arbitrary and time dependent, the density matrix satisfies the Liouville–von Neumann equation.

The variational approach will be illustrated in the next two sections.

### III. THE MODEL

The model represents an interacting  $N$  fermions system distributed in three levels or shells with degeneracy  $\mathcal{N} = N$ . The level energies are denoted by  $\varepsilon_k$  ( $k = 0, 1, 2$ ).

The particle states are characterized by two quantum numbers:  $k = 0, 1, 2$  which specifies the shell, and  $m = 1, 2, \dots, N$  which specifies the degenerate state within the shell. The Hamiltonian of the system is given by

$$H = \sum_{k=0}^2 \varepsilon_k \left[ \sum_{m=1}^N a_{km}^\dagger a_{km} \right] + \frac{1}{2} \sum_{k,l=0}^2 V_{kl} \sum_{m=1}^N \sum_{m'=1}^N a_{km}^\dagger a_{km'}^\dagger a_{lm'} a_{lm}, \quad (14)$$

where  $a_{km}^\dagger$  and  $a_{km}$  are the creation and annihilation fermionic operators of a particle at the level  $k$  in the state  $m$ . This is the most general definition of the model but, as usual in the literature, we consider the following restrictions (see for example [28] for a general discussion of the  $n$ -level LMG model):

- the levels are equally spaced and symmetrical around zero, i.e.,  $\varepsilon_2 = -\varepsilon_0 \equiv \varepsilon$  and  $\varepsilon_1 = 0$ ;
- we assume that the interaction does not scatter particles within the same level and that its strength is the same for all levels, i.e.,  $V_{kl} \equiv V(1 - \delta_{kl})$ .

We next define the operators

$$G_{ij} = \sum_{m=1}^N a_{im}^\dagger a_{jm}, \quad G_{ij}^\dagger = G_{ji}, \quad i, j = 0, 1, 2; \quad (15)$$

which are the nine generators of the  $U(3)$  group and satisfy the commutation relations

$$[G_{ij}, G_{kl}] = \delta_{jk} G_{il} - \delta_{il} G_{kj}. \quad (16)$$

If one takes into consideration that the particle number is a conserved quantity,  $N = G_{00} + G_{11} + G_{22}$ , eight is the number of independent operators, which are the generators of an  $SU(3)$  algebra. We can thus rewrite the Hamiltonian as

$$H = \varepsilon(G_{22} - G_{00}) + \frac{V}{2}(G_{01}^2 + G_{10}^2 + G_{02}^2 + G_{20}^2 + G_{12}^2 + G_{21}^2). \quad (17)$$

The scaled interaction parameter is defined in the usual way as

$$\chi = \frac{V(N-1)}{\varepsilon}. \quad (18)$$

The eigenstates of  $H$  are thus classified according to the irreducible representations of the  $SU(3)$  group and, as a consequence the hamiltonian matrix of order  $3^N$  splits into noninteracting blocks. This is due to the fact that the interaction does not change the label  $m$  of the scattered particle.

The second symmetry is due to the fact that the Hamiltonian scatters only *pairs* of particles, implying thus the conservation of the parity related to the shell's population. We therefore have

$$[H, \hat{\Pi}_1] = [H, \hat{\Pi}_2] = 0, \quad (19)$$

where

$$\hat{\Pi}_1 = \exp(i\pi G_{11}) \quad \text{and} \quad \hat{\Pi}_2 = \exp(i\pi G_{22}), \quad (20)$$

are parity operators. These symmetries allow for the classification of the states according to the parity of the eigenvalues of the diagonal operators (see ref. [23]).

#### IV. THE THERMODYNAMICS OF THE $SU(3)$ LIPKIN MODEL

We start by constructing the equilibrium density matrix as follows,

$$D_0 = K \exp(-\beta h_{MF}), \quad (21)$$

where

$$\begin{aligned} h_{MF} = & \alpha_1(G_{11} - G_{00}) + \alpha_2(G_{22} - G_{00}) + \alpha_3 G_{01} \\ & + \alpha_3^* G_{10} + \alpha_4 G_{02} + \alpha_4^* G_{20} + \alpha_5 G_{12} + \alpha_5^* G_{21}, \end{aligned} \quad (22)$$

where  $\alpha_1, \alpha_2 \in \mathbb{R}$ ,  $\alpha_3, \alpha_4, \alpha_5 \in \mathbb{C}$ , and  $K$  is the normalization constant. The eight variational parameters,  $\alpha_i$ , are obtained by minimizing the free energy, Eq. (9). As discussed before it is now convenient to work with  $D_0$  in diagonal form. For this purpose we write

$$D = UD_0U^\dagger = \frac{1}{Z} e^{\beta_1(G_{11} - G_{00})} e^{\beta_2(G_{22} - G_{00})}, \quad (23)$$

where

$$Z = z^N = \text{Tr}(e^{\beta_1(G_{11} - G_{00})} e^{\beta_2(G_{22} - G_{00})}), \quad (24)$$

$$U = U_3 U_2 U_1 = e^{is_3} e^{is_2} e^{is_1}, \quad (25)$$

with

$$\begin{aligned} s_1 &= z_1 G_{10} + z_1^* G_{01}, \\ s_2 &= z_2 G_{20} + z_2^* G_{02}, \end{aligned} \quad (26)$$

$$s_3 = z_3 G_{21} + z_3^* G_{12};$$

$$\beta_1, \beta_2 \in \mathbb{R} \quad \text{and} \quad z_1, z_2, z_3 \in \mathbb{C}. \quad (27)$$

The free energy is expressed as

$$\beta F = \beta \text{Tr}(DUHU^\dagger) + \text{Tr}(D \ln D). \quad (28)$$

We can thus calculate  $F$  as a function of the parameters. It is easy to check that the real parts of  $z_1$ ,  $z_2$  and  $z_3$  are irrelevant in what concerns the properties of stationary system *for attractive interactions* ( $\chi < 0$ ). This fact reduces the number of variational parameters to five real quantities:  $\theta_1 = iz_1$ ,  $\theta_2 = iz_2$ ,  $\theta_3 = iz_3$ ,  $\beta_1$  and  $\beta_2$ .

The free energy per particle can then be written as

$$\begin{aligned} \bar{F} = \frac{F}{N} = & -\cos(2\theta_2)(T_2 - \sin^2 \theta_3 T_3) + \frac{1}{2} \sin(2\theta_1) \sin \theta_2 \sin(2\theta_3) T_3 \\ & + \sin^2 \theta_1 (T_1 + \sin^2 \theta_3 T_3 - \sin^2 \theta_2 (T_2 - \sin^2 \theta_3 T_3)) \\ & + \frac{\chi}{4} \{ \cos^2 \theta_2 \sin^2(2\theta_3) T_3^2 + \sin^2(2\theta_2) (T_2 - \sin^2 \theta_3 T_3)^2 \\ & + \{ \sin(2\theta_1) (T_1 - \sin^2 \theta_2 T_2) + T_3 [ \sin(2\theta_1) (1 + \sin^2 \theta_2) \sin^2 \theta_3 \\ & + \cos(2\theta_1) \sin \theta_2 \sin(2\theta_3) ] \}^2 \} - \frac{1}{\beta} (\beta_1 T_1 + \beta_2 T_2 + \ln z), \end{aligned} \quad (29)$$

where

$$T_1 = \frac{\text{Tr}(D(G_{00} - G_{11}))}{N} = \frac{e^{-(\beta_1 + \beta_2)} - e^{\beta_1}}{z}, \quad (30)$$

$$T_2 = \frac{\text{Tr}(D(G_{00} - G_{22}))}{N} = \frac{e^{-(\beta_1 + \beta_2)} - e^{\beta_2}}{z}, \quad (31)$$

$$T_3 = \frac{\text{Tr}(D(G_{11} - G_{22}))}{N} = T_2 - T_1, \quad (32)$$

and

$$z = e^{\beta_1} + e^{\beta_2} + e^{-(\beta_1 + \beta_2)}. \quad (33)$$

The variational method requires

$$\frac{\partial \bar{F}}{\partial \theta_1} = \frac{\partial \bar{F}}{\partial \theta_2} = \frac{\partial \bar{F}}{\partial \theta_3} = \frac{\partial \bar{F}}{\partial \beta_1} = \frac{\partial \bar{F}}{\partial \beta_2} = 0. \quad (34)$$

This system of equations is given explicitly in Appendix A (Eqs. (134) to (137)). Its numerical analysis shows that the minimum conditions are satisfied when  $\theta_3 = 0$

TABLE I

Candidates to Minima of Free Energy Found Solving Equations (134)  
and (135) for  $\theta_3=0$  (or  $\pi$ )

$n$	$\theta_1$	$\theta_2$	$\chi$ range
1	0	0	—
2	0	$\frac{\pi}{2}$	—
3	0	$\frac{1}{2} \arccos\left(\frac{-2}{\chi T_2}\right)$	$ \chi  \geq 2$
4	$\frac{\pi}{2}$	0	—
5	$\frac{\pi}{2}$	$\frac{\pi}{2}$	—
6	$\frac{\pi}{2}$	$\frac{1}{2} \arccos\left(\frac{-1}{\chi T_2}\right)$	$ \chi  \geq 1$
7	—	$\frac{\pi}{2}$	$T_1 = T_2$
8	$\arcsin \sqrt{2 + \chi(T_2 - 2T_1)}$	$\arcsin \sqrt{T_1/T_2}$	$1 \leq \chi \leq 2$
9	$\frac{1}{2} \arccos\left(\frac{-1}{\chi T_1}\right)$	0	$ \chi  \geq 1$
10	$\frac{1}{2} \arccos\left(\frac{1}{\chi(T_2 - T_1)}\right)$	$\frac{\pi}{2}$	—
11	$\frac{1}{2} \arccos\left(\frac{3}{3 + 2\chi(T_2 - 2T_1)}\right)$	$\arcsin \sqrt{\frac{3 + \chi(2T_2 - T_1)}{3\chi T_2}}$	$ \chi  \geq 3$

or  $\pi$ . This is very fortunate, since with this (numerical) result we can obtain analytic expressions for the solutions  $\theta_1$  and  $\theta_2$  as a function of the coupling strength and the temperature. They are presented in Table I.

The solutions presented in the table are then substituted in Eqs. (137) and the parameters  $\beta_1$  and  $\beta_2$  are found numerically. We verify that the solutions which correspond to minima are three (1, 9 and 11 in Table I), each one of them valid for different intervals of  $\chi$  and  $\beta$ . They are:

- *Strong Coupling Regime (SCR)*: Occurring for  $\chi \leq -3$  and  $\beta \geq \beta_{cr1}$ , where  $\beta_{cr1}$  is found numerically and displayed in the figures. These conditions are summarized by

$$\chi T_1 \leq -3. \quad (35)$$

The parameters in this case are

$$\beta_1 = \beta_2 \Rightarrow T_1 = T_2 = T, \quad (T_3 = 0), \quad (36)$$

$$\cos(2\theta_1) = \frac{3}{3 - 2\chi T}, \quad \sin^2 \theta_2 = \frac{3 + \chi T}{3\chi T}, \quad \theta_3 = 0. \quad (37)$$

• *Intermediate Coupling Regime (ICR)*: Occurring for  $\chi \leq -1$  and temperature interval that has to be found numerically

$$\beta_{cr2} \leq \beta \leq \beta_{cr1} \quad \text{for } \chi \leq -3, \quad (38)$$

$$\beta \geq \beta_{cr2} \quad \text{for } -3 \leq \chi \leq -1, \quad (39)$$

or in more compact form

$$-3 \leq \chi T_1 \leq -1. \quad (40)$$

The parameters are

$$\cos(2\theta_1) = -\frac{1}{\chi T_1}, \quad \theta_2 = 0, \quad \theta_3 = 0. \quad (41)$$

• *Weak Coupling Regime (WCR)*: Occurring for all values of  $\chi$  being a minimum when

$$\beta \leq \beta_{cr2} \quad \text{for } \chi \leq -1 \quad (42)$$

and

$$\forall \beta \quad \text{for } -1 \leq \chi \leq 0, \quad (43)$$

or in more compact form

$$\chi T_1 \geq -1. \quad (44)$$

The parameters are

$$\theta_1 = \theta_2 = \theta_3 = 0, \quad \beta_1 = 0, \quad \beta_2 = -\beta. \quad (45)$$

The phase transition temperatures are found numerically and the analytical expressions defining them are  $\chi T_1 = -1$  and  $\chi T_1 = -3$ . We thus conclude that the state of statistical equilibrium is determined by the parameter  $\chi' = \chi T_1$ . The weak coupling phase, as discussed in the introduction corresponds to a regime where the coupling strength plays no role in the definition of the equilibrium state. It corresponds to an extremum of the free energy for any value of  $\chi$  and therefore it is a physical situation corresponding to high temperatures or weak enough coupling. The SCR

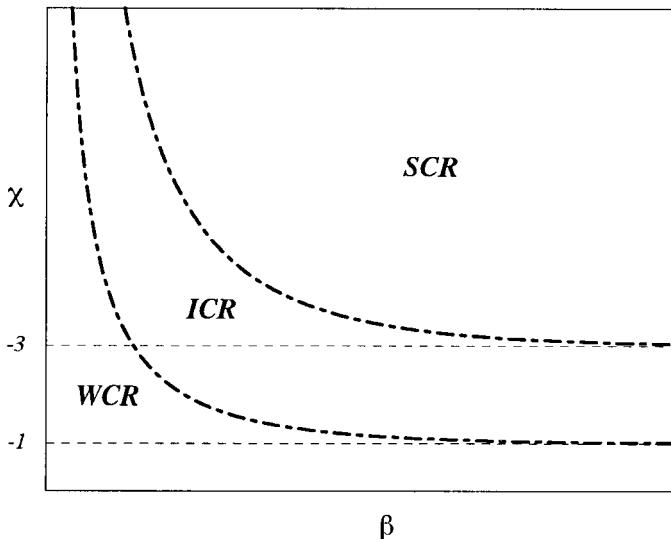


Fig. 1. Phase diagram  $\chi \times \beta$  of the model. The relations between  $\chi$  and the inverse of the phase transition temperatures are shown schematically by thick dot-dashed lines. The three phases regions are indicated as well as the minimum values of  $\chi$  for the SCR and ICR existence (thin dashed lines).

corresponds to the situation where the interaction prevails for characterization of the equilibrium density. In this case we may think that the dynamical coupling is present in all three levels of the model since the parameters  $\theta_1$  and  $\theta_2$  are non zero. The ICR is, in fact, an intermediate situation, since in this case the interaction is only effective in the lower levels. Figure 1 shows schematically the relation between  $\chi$  and  $\beta$ . The phase transition lines are just sketched.

#### IV.1. Thermodynamical Properties

In this section we present a detailed analysis of the relevant thermodynamical quantities which allow for a characterization of the three phases of the system.

We start by showing the free energy as a function of  $\beta$  for three values of the coupling strength in Figs. 2(a-c). In Fig. 2(a),  $\chi = -6.0$  and, as we see, the three solutions are present and correspondingly two phase transitions: the first one, from SCR to ICR occurs for  $\beta_{cr1} = 0.4621$  and the second one, from ICR to WCR, in  $\beta_{cr2} = 0.4258$ . In Fig. 2(b) which corresponds to a smaller  $\chi$  value, we find only one phase transition (from ICR to WCR). In this case the SCR does not exist. Figure 2(c) does not show any phase transition. The WCR solution is the only one.

The entropy and the internal energy are shown in Fig. 3 for  $\chi = -6.0$ . Although they are continuous, none of them is analytical at the critical temperature. For low temperatures the entropy is very small and the free energy is dominated by the

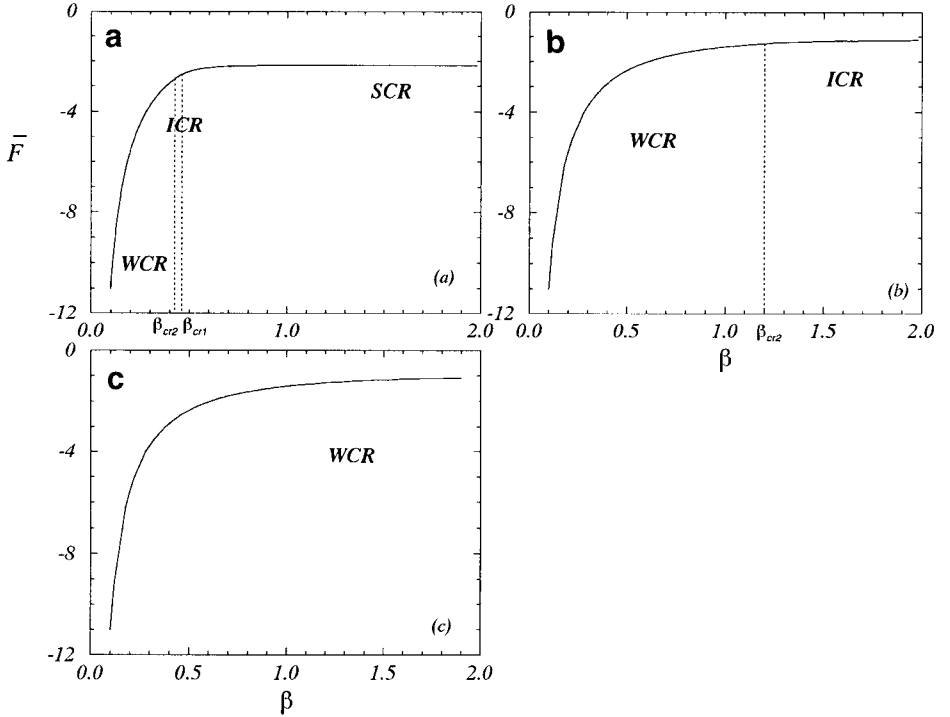


Fig. 2. Free energy  $\bar{F}$  as function of inverse temperature  $\beta$  for three different values of coupling parameter (a)  $\chi = -6.0$ , (b)  $\chi = -2.0$  and (c)  $-1 \leq \chi \leq 0$ . Note that in (a) there are three phases (they are separated by a vertical dotted line), in (b) two phases and in (c) just one phase. The critical inverse temperatures are indicated.

contribution of the internal energy. As the temperature grows this is reversed, as expected.

Another quantity which turns out to be very instructive is the average value of the level's population difference as a function of  $\chi$  and  $\beta$ , namely

$$P_{01} = \frac{\langle T_1 \rangle}{N} = \frac{\text{Tr}(DU(G_{00} - G_{11}) U^\dagger)}{N} = \cos(2\theta_1)(T_1 + \sin^2 \theta_3 T_3 - \sin^2 \theta_2(T_2 - \sin^2 \theta_3 T_3)) + \sin(2\theta_1) \sin \theta_2 \sin(2\theta_3) T_3, \quad (46)$$

$$P_{02} = \frac{\langle T_2 \rangle}{N} = \frac{\text{Tr}(DU(G_{00} - G_{22}) U^\dagger)}{N} = \cos(2\theta_2)(T_2 - \sin^2 \theta_3 T_3) - \frac{1}{2} \sin(2\theta_1) \sin \theta_2 \sin(2\theta_3) T_3 - \sin^2 \theta_1(T_1 + \sin^2 \theta_3 T_3 - \sin^2 \theta_2(T_2 - \sin^2 \theta_3 T_3)), \quad (47)$$

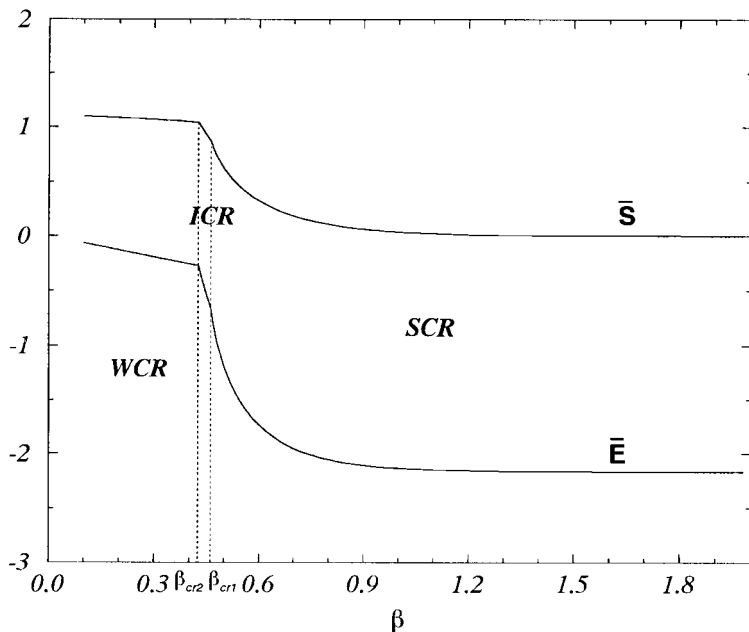


Fig. 3. Internal energy  $\bar{E}$  and entropy  $\bar{S}$  as function of inverse temperature for  $\chi = -6.0$ . The values of critical inverse temperatures  $\beta_{cr1}$  and  $\beta_{cr2}$  are indicated.

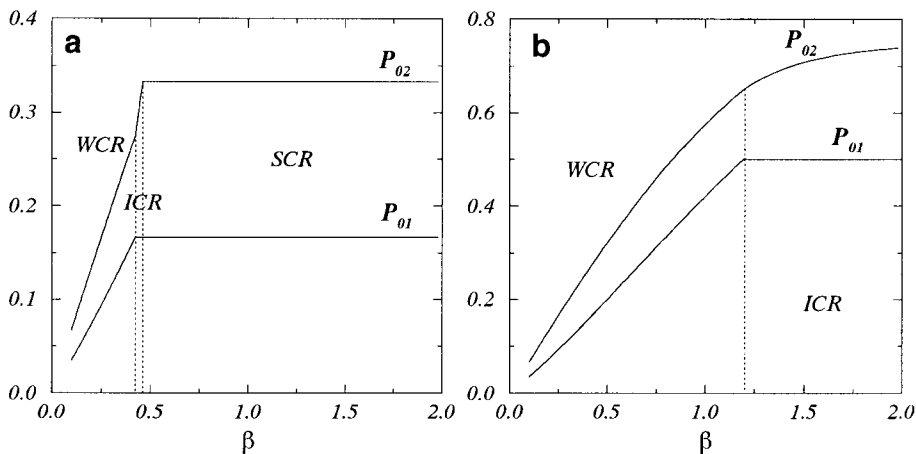


Fig. 4.  $P_{01}$  and  $P_{02}$  as function of inverse temperature  $\beta$  for two values of coupling parameter (a)  $\chi = -6.0$  and (b)  $\chi = -2.0$ .

where  $P_{01(02)}$  is the average of the population difference between the first (second) and the lowest level. They are shown in Fig. 4(a) and (b). For the strong coupling regime both population differences are held constant up to  $\beta = \beta_{cr1}$ . This clearly reveals the dominant role played by the coupling strength in this thermodynamic phase. For  $\beta_{cr2} \leq \beta \leq \beta_{cr1}$  we see that the temperature effectively attenuates this role of  $\chi$ . In this case the population difference between levels 0 and 2 decreases, while the difference between 0 and 1 is the same as before. Below  $\beta_{cr2}$  the interaction effects are completely absent and the system will tend to populate equally all levels as required by entropy maximization. We thus conclude that increasing the temperature tends to effectively “weaken” the dynamical coupling.

The two phase transitions of the system are clearly reflected in the system’s specific heat, as shown in Fig. 5. The behavior of the order parameters are shown in Fig. 6. The average values of the operators  $(G_{02} + G_{20})/2$  and  $(G_{01} + G_{10})/2$  may be chosen as order parameters of the first ( $SCR \rightarrow ICR$ ) and the second ( $ICR \rightarrow WCR$ ) phase transitions respectively. We have

$$\langle G_{01} \rangle = \langle G_{10} \rangle = -\frac{\sin(2\theta_1)}{2} (T_1 - \sin^2 \theta_2 T_2), \quad (48)$$

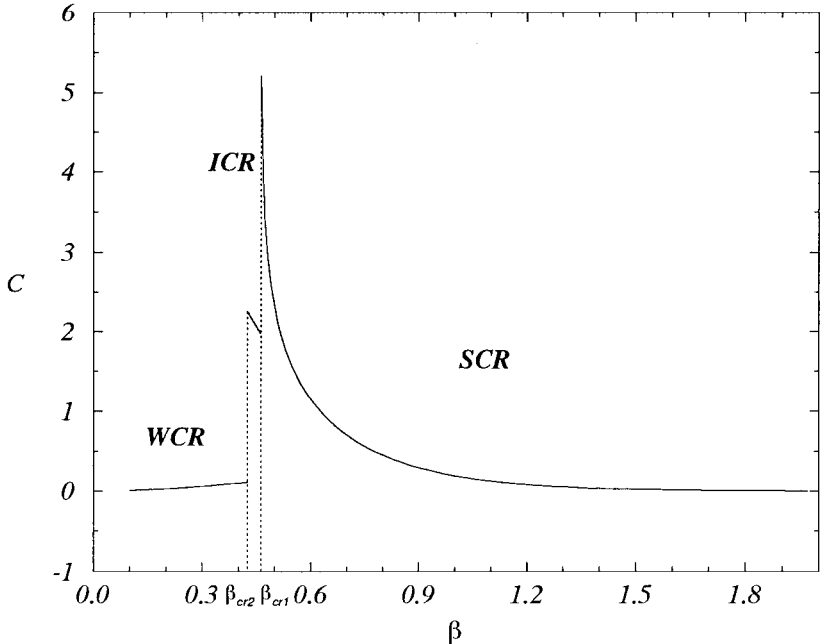


Fig. 5. The specific heat of the system as function of  $\beta$  for  $\chi = -6.0$ . Note the two second order phase transitions.

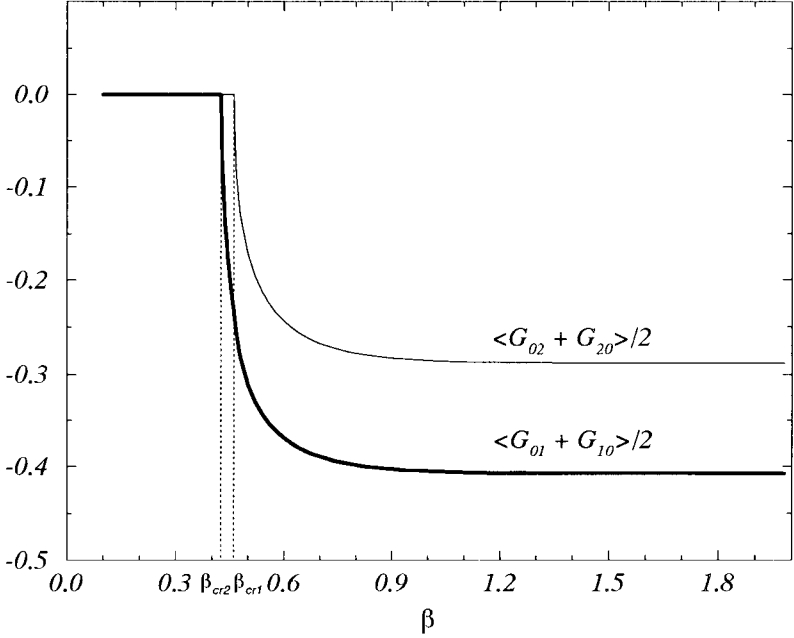


Fig. 6. Order parameters  $\langle G_{02} + G_{20} \rangle / 2$  and  $\langle G_{01} + G_{10} \rangle / 2$  of the *SCR*  $\rightarrow$  *ICR* and *ICR*  $\rightarrow$  *WCR* phase transitions respectively as function of the inverse temperature  $\beta$  for  $\chi = -6.0$ .

and

$$\langle G_{02} \rangle = \langle G_{20} \rangle = -\frac{\cos(\theta_1) \sin(2\theta_2)}{2} T_2. \quad (49)$$

Their interpretations again show the suppression of the particle's transitions due to the dynamics involving level 2 (first phase transition) and level 1 (second phase transition).

We also calculated the average values of the Casimir operators of second order and third order scaled by  $N^2$  and  $N^3$  respectively

$$\langle C_2 \rangle = \frac{1}{N^2} \sum_{i,j} \text{Tr}(DG_{ij}G_{ji}), \quad (50)$$

$$\langle C_3 \rangle = \frac{1}{N^3} \sum_{i,j,k} \text{Tr}(DG_{ij}G_{jk}G_{ki}). \quad (51)$$

Their values depend only on  $\beta$  and  $\chi$  and are completely independent of the state choice. We notice that, when the temperature is zero, the values of  $\langle C_2 \rangle$  and  $\langle C_3 \rangle$  are always equal to 1, which corresponds to the value of the Casimir operators in

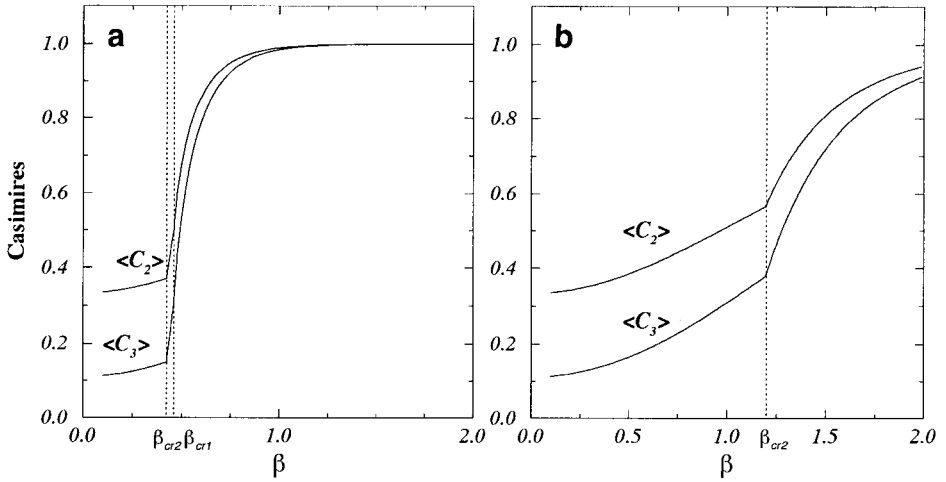


Fig. 7. Scaled average values of the Casimir operators  $\langle C_2 \rangle$  and  $\langle C_3 \rangle$  as function of  $\beta$  for (a)  $\chi = -6.0$  and (b)  $\chi = -2.0$ .

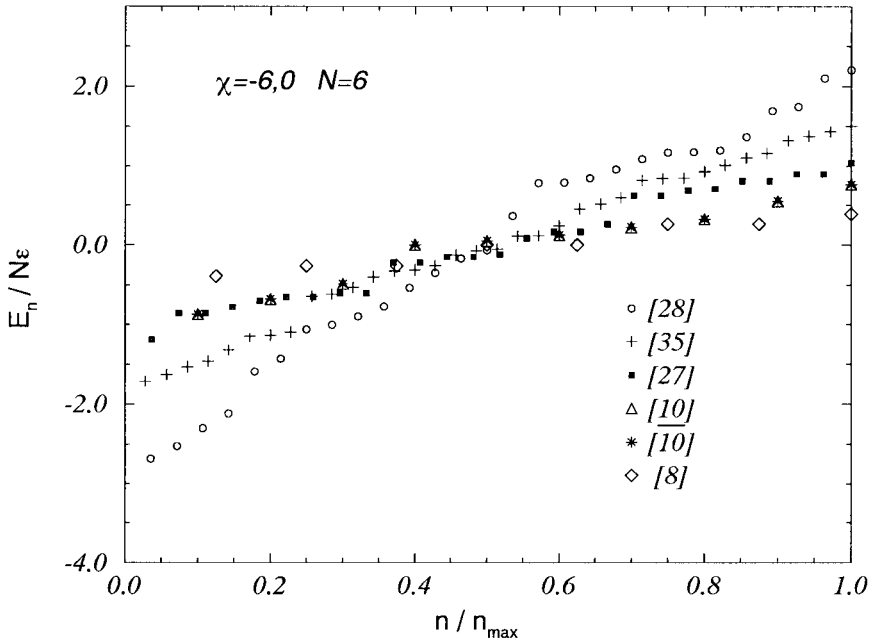


Fig. 8. All the eigenvalues of energy  $E_n/N\varepsilon$  versus  $n/n_{max}$  for  $\chi = -6.0$  and  $N=6$ . They are separated according to the irreducible representations they belong to (see Fig. 9). The quantity  $n_{max}$  is the number of eigenstates of each irreducible representation and it is used to label it. Besides  $n = 1, \dots, n_{max}$ .

the symmetric representation. As temperature grows, these average values decrease which would correspond, in the quantum context, to the contribution to the statistical averages of states belonging to other representations. We see from Fig. 7(a) that for  $\chi \leq -3$  this occurs in a temperature range which is below but close to the  $SCR \rightarrow ICR$  phase transition. Now, for systems with  $-3 \leq \chi \leq 0$ , this occurs for any finite temperature. This is shown in Fig. 7(b).

#### IV.2. Exact Thermodynamic Calculation: Finite $N$ Results

The mean field approximation used in the present work involves all the different irreducible representations of the  $SU(3)$  group. It is possible to investigate their role in an exact calculation for finite  $N$ . For example, in Fig. 8 we display the eigenvalues of the Hamiltonian (17) for  $N=6$  and  $\chi = -6.0$ . They are separated according to the irreducible representations they belong to. The  $3^6$  states are distributed in the various representations in the following way,

$$[3] \otimes [3] \otimes [3] \otimes [3] \otimes [3] \otimes [3] = [28] \oplus 5 \times [35] \oplus 9 \times [27] \oplus 10 \times [10] \\ \oplus 5 \times [\bar{10}] \oplus 16 \times [8] \oplus 5 \times [1], \quad (52)$$

where the symbols in brackets correspond to the representation illustrated in Fig. 9.

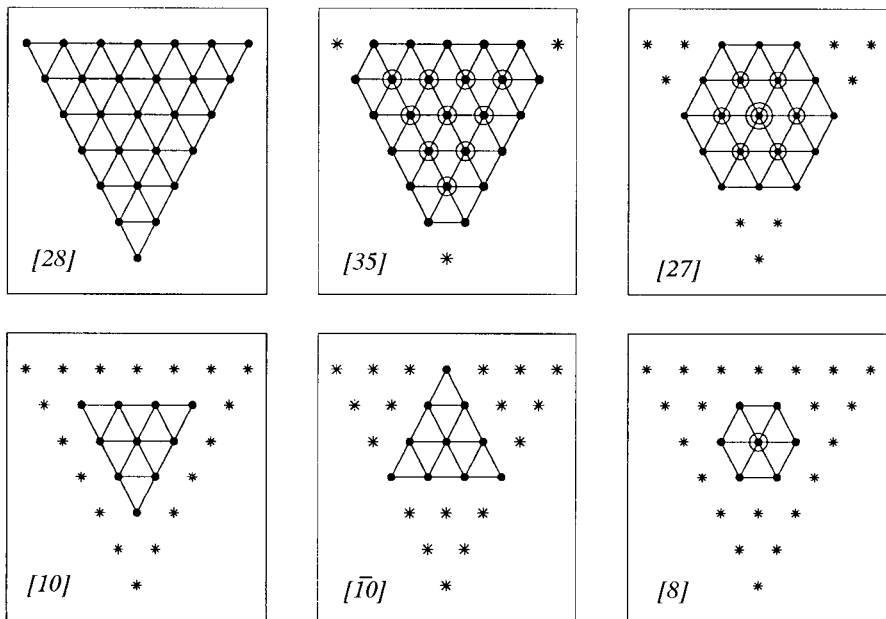


Fig. 9. Irreducible representations of a 6 particles system. The stars show the positions which are not occupied by states in the antisymmetric representations while the circumcentric circles indicate the number of states which occupy the same position in the diagram.

We are now in a position to calculate the relative contribution of the various irreducible representations as a function of temperature. For this purpose we define

$$P_{[a]} = \sum_{E_j \in [a]} Y_{[a]} \frac{\exp(-\beta E_j)}{Z}, \quad (53)$$

where  $Y_{[a]}$  is the multiplicity factor of the representation  $[a]$ .

In Fig. 10 we show  $P_{[a]}$  as a function of inverse temperature for  $N=6$  and  $\chi = -6.0$ . The three phases regions are separated by the vertical thick dot-dashed lines. We see that for the strong coupling regime the main contribution comes from the symmetric representation ( $[28]$ ). As the temperature increases the other irreducible representations start to give nonnegligible contributions. This result is consistent with the mean field average values of the Casimir operators, as we saw in Fig. 7.

In order to illustrate the adequacy of the m.f.a. we compare the exact and mean field results. In Fig. 11, we show the free energy obtained by mean field approximation and exact calculation for  $N=4$  and  $N=6$ , where we have considered all irreducible representations states and  $N=30$ , where we considered only the symmetric representation states. The numerical calculation for exact quantities that computes all accessible states is rather involved, therefore we have stopped at  $N=6$ .

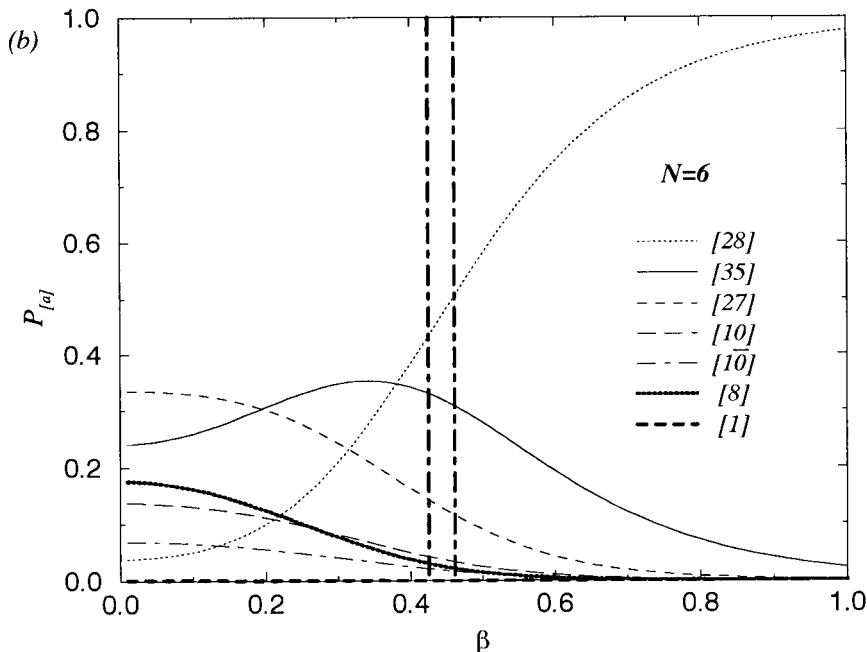


Fig. 10. Relative contribution of the irreducible representations  $P_{[a]}$  for  $N=6$  and  $\chi = -6.0$  as function of inverse temperature  $\beta$ . The vertical thick dot-dashed lines separate the three phases regions.

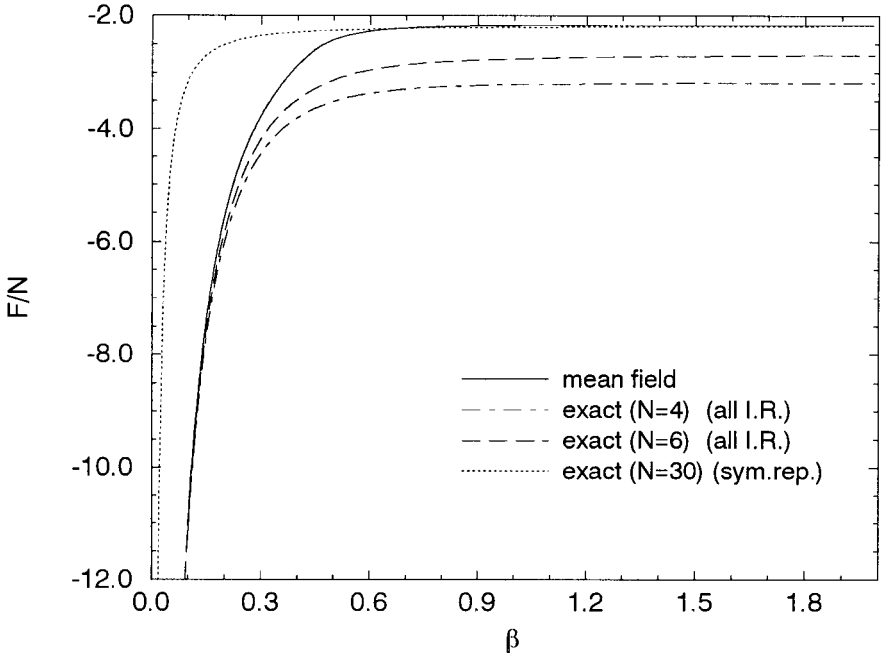


Fig. 11. Mean field result (solid line) and exact results obtained considering all  $3^N$  states for  $N=4$  (dot-dashed line),  $N=6$  (dashed line) for the average free energy  $\bar{F}$  as function of inverse temperature  $\beta$  for  $\chi = -6.0$ . The dotted line represents the result for 30 particles, but just considering the symmetric representation states. We can observe that for SCR this representation is the main responsible for the system behavior.

However, it is possible to observe, even for small  $N$ , the convergence of the exact curves toward the mean field one. For low enough temperatures, when the symmetric representation alone dominates the behavior of the system, it is seen that the dotted line agrees very well with the mean field curve.

## V. FINITE TEMPERATURE EFFECTS IN THE CLASSICAL DYNAMICS

We start by introducing the thermal classical Lagrangian of the system ( $\hbar = 1$ ),

$$L = i \text{Tr}(DU\dot{U}^\dagger) - \text{Tr}(DUHU^\dagger), \quad (54)$$

where  $D$  is the equilibrium diagonal density given by Eq. (23) and  $U$  has the same form as in the previous section, but with time dependent parameters, that is,

$$U = U_3 U_2 U_1 = e^{is_3(t)} e^{is_2(t)} e^{is_1(t)}, \quad (55)$$

with

$$s_1(t) = z_1(t) G_{10} + z_1^*(t) G_{01}, \quad (56)$$

$$s_2(t) = z_2(t) G_{20} + z_2^*(t) G_{02}, \quad (57)$$

$$s_3(t) = z_3(t) G_{21} + z_3^*(t) G_{12}. \quad (58)$$

The definition of classical variables comes from the first term on the r.h.s. of Eq. (54). We get

$$\begin{aligned} \frac{\text{Tr}(DU\dot{U}^\dagger)}{N} &= \frac{\dot{z}_3 z_3^* - z_3 \dot{z}_3^*}{2 R_3^2} S_3^2 T_3 + \frac{\dot{z}_2 z_2^* - z_2 \dot{z}_2^*}{2 R_2^2} S_2^2 (T_2 - S_3^2 T_3) \\ &+ \frac{\dot{z}_1 z_1^* - z_1 \dot{z}_1^*}{2 R_1^2} S_1^2 \left\{ T_1 + S_3^2 T_3 - S_2^2 (T_2 - S_3^2 T_3) \right. \\ &+ \left. i \frac{(z_1 z_2^* z_3 - z_1^* z_2 z_3^*)}{R_1 R_2 R_3} \frac{C_1 S_2 S_3 C_3}{S_1} T_3 \right\} \\ &+ i \frac{(\dot{z}_1 z_1^* + z_1 \dot{z}_1^*)}{2 R_1^2} (z_1 z_2^* z_3 + z_1^* z_2 z_3^*) \frac{S_2 S_3 C_3}{R_2 R_3} T_3 \end{aligned} \quad (59)$$

with

$$S_j = \sin \sqrt{z_j z_j^*}, \quad C_j = \cos \sqrt{z_j z_j^*}, \quad R_j = \sqrt{z_j z_j^*}, \quad j = 1, 2, 3. \quad (60)$$

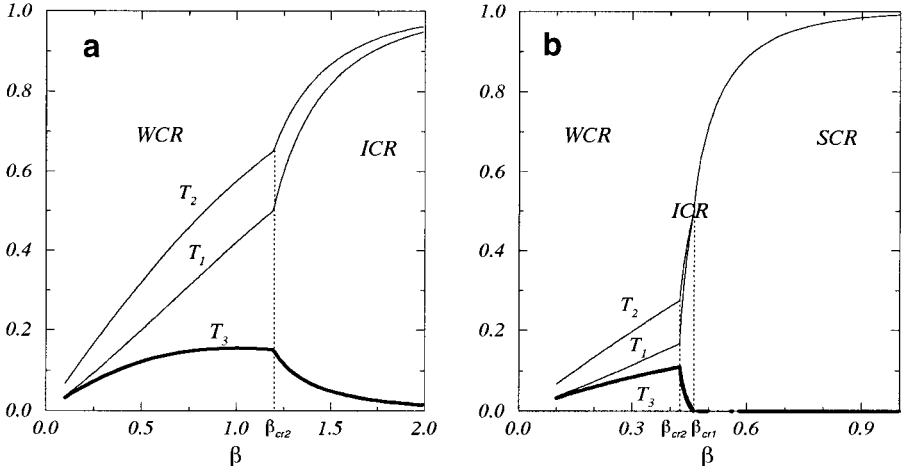


Fig. 12. Plot of  $T_1$ ,  $T_2$  and  $T_3$  as function of  $\beta$  for  $\chi = -6.0$ . Note that in the SCR,  $T_3$  vanishes and  $T_1$  and  $T_2$  have the same value.

The quantities  $T_1$ ,  $T_2$  and  $T_3$ , given by (30) to (32), are very important in the study of the dynamics. They have been obtained in the previous section for attractive interaction ( $\chi < 0$ ) and are displayed in Fig. 12 as function of inverse temperature for (a)  $\chi = -2$  and (b)  $\chi = -6$ .

In principle for an arbitrary initial condition ( $\beta_1$  and  $\beta_2$ ) we have three pairs of noncanonical variables. We may choose  $\beta_1$  and  $\beta_2$  of the thermodynamical equilibrium state. The second term on the r.h.s. of Eq. (54) is the classical counterpart of the quantum Hamiltonian of the system defined in Section III. In terms of the variables  $z_1$ ,  $z_2$  and  $z_3$  it is given by

$$\begin{aligned}
\frac{\mathcal{H}(z_i, z_i^*)}{N} = & (-1 + 2S_2^2)(T_2 - S_3^2 T_3) + i(z_1 z_2^* z_3 - z_1^* z_2 z_3^*) \frac{S_1 C_1 S_2 S_3 C_3}{R_1 R_2 R_3} T_3 \\
& + S_1^2 \{ T_1 + S_3^2 T_3 - S_2^2 (T_2 - S_3^2 T_3) \} + \frac{\chi}{2} \left\{ -(z_1^2 + z_1^{*2}) \left( \frac{S_1 C_1}{R_1} \right)^2 \right. \\
& \cdot \{ T_1 + S_3^2 T_3 - S_2^2 (T_2 - S_3^2 T_3) \}^2 + \left\{ [(z_2 z_3^*)^2 + (z_2^* z_3)^2] C_1^4 \right. \\
& + \left. \left[ \left( \frac{z_1 z_2^* z_3}{z_1^*} \right)^2 + \left( \frac{z_1^* z_2 z_3^*}{z_1} \right)^2 \right] S_1^4 + 2 \left( \frac{z_1}{z_1^*} + \frac{z_1^*}{z_1} \right) R_2^2 R_3^2 C_1^2 S_1^2 \right\} \\
& \cdot \left( \frac{S_2 S_3 C_3}{R_2 R_3} \right)^2 T_3^2 + \left\{ (z_1 z_2 z_3^* - z_1^* z_2^* z_3) C_1^2 + \left( \frac{z_1^2 z_2^* z_3}{z_1^*} - \frac{z_1^{*2} z_2 z_3^*}{z_1} \right) S_1^2 \right\} \\
& \cdot 2i \frac{S_1 C_1 S_2 S_3 C_3}{R_1 R_2 R_3} T_3 [T_1 + S_3^2 T_3 - S_2^2 (T_2 - S_3^2 T_3)] - (z_2^2 + z_2^{*2}) \\
& \cdot \left( \frac{C_1 S_2 C_2}{R_2} \right)^2 (T_2 - S_3^2 T_3)^2 + [(z_1 z_3)^2 + (z_1^* z_3^*)^2] \left( \frac{S_1 C_2 S_3 C_3}{R_1 R_3} \right)^2 T_3^2 \\
& - 2i(z_1 z_2 z_3 - z_1^* z_2^* z_3^*) \frac{S_1 C_1 S_2 C_2^2 S_3 C_3}{R_1 R_2 R_3} T_3 (T_2 - S_3^2 T_3) - (z_3^2 + z_3^{*2}) \\
& \cdot \left( \frac{C_1 C_2 S_3 C_3}{R_3} \right)^2 T_3^2 + [(z_1^* z_2)^2 + (z_1 z_2^*)^2] \left( \frac{S_1 S_2 C_2}{R_1 R_2} \right)^2 [T_2 - S_3^2 T_3]^2 \\
& \left. - 2i(z_1^* z_2 z_3 - z_1 z_2^* z_3^*) \frac{S_1 C_1 S_2 C_2^2 S_3 C_3}{R_1 R_2 R_3} T_3 (T_2 - S_3^2 T_3) \right\}. \quad (61)
\end{aligned}$$

At this point we tried to express the three degrees of freedom of our system in terms of canonical variables. At this point we tried to express the three degrees of freedom of our system in terms of canonical variables. However, in spite of Darboux's theorem which guarantees the existence of canonical forms [1] we have not succeeded in obtaining useful analytical expressions, except for the SCR. In this case the classical dynamics of the system reduces to two degrees of freedom as in the zero temperature

case. In the other regimes we have an important temperature effect in the classical dynamics of the model: the appearance of a third degree of freedom, which does not exist at zero temperature. In order to study this novel effect we will first restrict ourselves to the small amplitude regime of the dynamics where all results are analytical. This was done in reference [38]. We give a brief summary of the main results.

### V.1. Small Amplitude Motion

The small amplitude fluctuations around equilibrium are described by the second order Lagrangian

$$\mathcal{L}^{(2)} = \sum_{j=1}^3 \frac{i}{2} (\dot{\gamma}_j \gamma_j^* - \gamma_j \dot{\gamma}_j^*) - \mathcal{H}^{(2)}(\gamma_j, \gamma_j^*), \quad (62)$$

with

$$\mathcal{H}^{(2)}(\gamma_j, \gamma_j^*) = \frac{1}{2} \begin{pmatrix} \gamma_1^* & \gamma_2^* & \gamma_3^* & \gamma_1 & \gamma_2 & \gamma_3 \end{pmatrix} \begin{pmatrix} A & B \\ B & A \end{pmatrix} \begin{pmatrix} \gamma_1 \\ \gamma_2 \\ \gamma_3 \\ \gamma_1^* \\ \gamma_2^* \\ \gamma_3^* \end{pmatrix}, \quad (63)$$

where the variables  $\gamma_j, \gamma_j^*, j=1, 2, 3$  are canonical variables related to the small deviations,  $\delta z_j, \delta z_j^*$ , from the equilibrium solution and  $A, B$  are  $3 \times 3$  matrices which are defined according to the different phases. From now on we present the small amplitude motion around the thermodynamical equilibrium solution in each one of the three possible regimes. The RPA frequencies  $\Omega_j$  [39], i.e., the small amplitude frequencies are determined from the equation

$$\Omega_j^2 u = (A + B) \cdot (A - B) u, \quad j = 1, 2, 3. \quad (64)$$

where  $u$  are the RPA eigenvectors. We obtain the following RPA frequencies:

1. *Weak coupling regime* ( $\chi T_1 \geq -1$ ):

$$\Omega_1 = \sqrt{1 - \chi^2 T_1^2}, \quad \Omega_2 = \sqrt{4 - \chi^2 T_2^2}, \quad \Omega_3 = \sqrt{1 - \chi^2 T_3^2}. \quad (65)$$

2. *Intermediate coupling regime* ( $-3 \leq \chi T_1 \leq -1$ ):

$$\Omega_1 = \sqrt{2[(\chi T_1)^2 - 1]}, \quad (66)$$

$$\Omega_2 = \frac{1}{2} \sqrt{(3 - \chi T_1)^2 - (2\chi T_2)^2}, \quad (67)$$

$$\Omega_3 = \frac{1}{2} \sqrt{(3 + \chi T_1)^2 - (2\chi T_3)^2}. \quad (68)$$

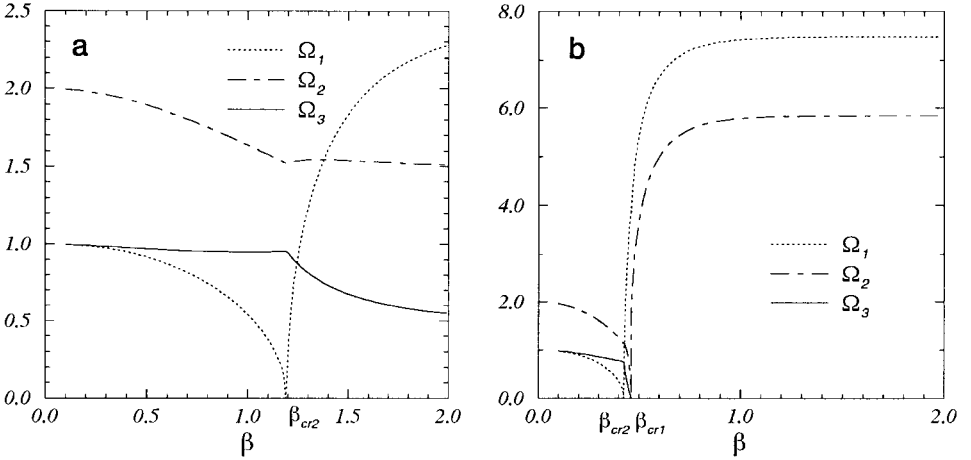


Fig. 13. RPA frequencies as function of the inverse temperature  $\beta$  of the system for (a)  $\chi = -2.0$  and (b)  $\chi = -6.0$ . Note the “awakening” of the third mode in the SCR  $\rightarrow$  ICR phase transition.

### 3. Strong coupling regime ( $\chi T_1 \leq -3$ ):

There are only two modes:

$$\Omega_i = \sqrt{\frac{4}{3}[(T_1\chi)^2 - 3 \pm \sqrt{9 + 3(T_1\chi)^2}]}, \quad i = 1, 2. \quad (69)$$

In the limit of zero temperature,  $T_3 \rightarrow 0$ ,  $T_i \rightarrow 1$ ,  $i = 1, 2$ , the RPA frequencies reduce to the ones given in ref. [22],

$$i = 1, 2 \quad \Omega_i = \begin{cases} \sqrt{1 - \chi^2}, \sqrt{4 - \chi^2}, & -1 < \chi < 0 \\ \sqrt{2(\chi^2 - 1)}, \frac{1}{2}\sqrt{3(\chi + 3)(1 - \chi)}, & -3 < \chi < -1 \\ \sqrt{\frac{4}{3}[\chi^2 - 3 \pm \sqrt{3\chi^2 + 9}]}, & \chi < -3. \end{cases}$$

In Fig. 13(a) and (b) the RPA frequencies are represented respectively for  $\chi = -2$  and  $\chi = -6$ .

We notice that for finite temperatures the third mode is excited whereas it remains inert for zero temperature and also for the strong coupling regime. This feature of temperature dependence of small frequency modes is also described in ref. [40].

## V.2. Large Amplitude Motion in the SCR

As aforementioned, in the SCR the term  $T_3$  vanishes and the classical dynamics is restricted to two degrees of freedom. We are then able to find two pairs of canonically conjugate variables and to completely analyze the dynamics of the system including their stationary points in an analogous way to ref. [24] and characterize the classical

trajectories in all phase space. Therefore, *for this phase* we define the pairs of canonically conjugate variables

$$\gamma_1 = z_1 \frac{\sin \sqrt{z_1 z_1^*}}{\sqrt{z_1 z_1^*}} \cos \sqrt{z_2 z_2^*} \sqrt{T}, \quad (70)$$

$$\gamma_2 = z_2 \frac{\sin \sqrt{z_2 z_2^*}}{\sqrt{z_2 z_2^*}} \sqrt{T} \quad (T_1 = T_2 \equiv T). \quad (71)$$

Note that  $T$  does not stand for temperature from now on.

In terms of these variables Eq. (59) reduces to

$$\frac{\text{Tr}(DU\dot{U}^\dagger)}{N} = \frac{1}{2} \sum_{i=1}^2 \dot{\gamma}_i \gamma_i^* - \gamma_i \dot{\gamma}_i^*, \quad (72)$$

and the classical Hamiltonian is given by

$$\begin{aligned} \mathcal{H}_{cl} = & -T + 2\gamma_2 \gamma_2^* + \gamma_1 \gamma_1^* + \frac{\chi}{2} \{ -(T - \gamma_1 \gamma_1^* - \gamma_2 \gamma_2^*) \\ & \times (\gamma_1^2 + \gamma_1^{*2} + \gamma_2^2 + \gamma_2^{*2}) + (\gamma_1^* \gamma_2)^2 + (\gamma_1 \gamma_2^*)^2 \}. \end{aligned} \quad (73)$$

One of the temperature effects on this dynamics is to restrict the phase space of the system (see Eq. (70) and (71))

$$0 \leq \gamma_2 \gamma_2^* \leq T \quad (74)$$

and

$$0 \leq \frac{\gamma_1 \gamma_1^*}{T - \gamma_2 \gamma_2^*} \leq 1. \quad (75)$$

We found it convenient to express the classical Hamiltonian in terms of the new variables

$$\gamma_2 = \sqrt{\eta_2} e^{i\theta_2} \quad \text{and} \quad \gamma_1 = \sqrt{\eta_1} e^{i\theta_1}, \quad (76)$$

with the range of allowed values

$$0 \leq \eta_1 + \eta_2 \leq T. \quad (77)$$

In the large  $N$  limit (classical limit) the classical scaled Hamiltonian is defined as

$$\begin{aligned} E = \frac{\mathcal{H}_{cl}}{N} = & -T + 2\eta_2 + \eta_1 + \chi \{ -(T - \eta_1 - \eta_2) [\eta_1 \cos(2\theta_1) + \eta_2 \cos(2\theta_2)] \\ & + \eta_1 \eta_2 \cos[2(\theta_1 - \theta_2)] \}. \end{aligned} \quad (78)$$

In the limit of zero temperature we recover the result previously obtained in ref. [24], (see Eq. (2.9)). Also when  $\eta_2=0$  we recover the finite temperature  $SU(2)$  result [37].

Our variables  $\eta_1$  and  $\eta_2$  correspond to the action variables of the free system and are related to the population  $N_k$  of the levels scaled by the number of particles

$$N_1 = \frac{\text{Tr}(DUG_{11}U^\dagger)}{N} = \frac{\text{Tr}(DG_{11})}{N} + \eta_1, \quad (79)$$

$$N_2 = \frac{\text{Tr}(DUG_{22}U^\dagger)}{N} = \frac{\text{Tr}(DG_{22})}{N} + \eta_2, \quad (80)$$

$$N_0 = \frac{\text{Tr}(DUG_{00}U^\dagger)}{N} = \frac{\text{Tr}(DG_{00})}{N} - \eta_1 - \eta_2. \quad (81)$$

The allowed range for these variables is a consequence of the conservation of the number of particles ( $\sum_{k=0}^2 N_k = 1$ ). We could have as well used  $N_k$  instead of  $\eta_k$ . This would, however increase the number of terms in the classical Hamiltonian. Alternatively we can define new temperature independent variables

$$\Gamma_1 = \frac{\gamma_1}{\sqrt{T}} = z_1 \frac{\sin \sqrt{z_1 z_1^*}}{\sqrt{z_1 z_1^*}} \cos \sqrt{z_2 z_2^*} \Rightarrow \mathcal{J}_1 = \frac{\eta_1}{T}, \quad (82)$$

$$\Gamma_2 = \frac{\gamma_2}{\sqrt{T}} = z_2 \frac{\sin \sqrt{z_2 z_2^*}}{\sqrt{z_2 z_2^*}} \Rightarrow \mathcal{J}_2 = \frac{\eta_2}{T}, \quad (83)$$

and an effective coupling constant

$$\chi_\beta = \chi T, \quad (84)$$

which leads to

$$\frac{L}{N} = T \frac{i}{2} \sum_{k=1}^2 (\dot{\Gamma}_k \Gamma_k^* - \Gamma_k \dot{\Gamma}_k^*) - T \mathcal{E}, \quad (85)$$

where

$$\begin{aligned} \mathcal{E} = \frac{E}{T} = & -1 + 2\mathcal{J}_2 + \mathcal{J}_1 + \chi_\beta \{ -(1 - \mathcal{J}_1 - \mathcal{J}_2)[\mathcal{J}_1 \cos(2\theta_1) \\ & + \mathcal{J}_2 \cos(2\theta_2)] + \mathcal{J}_1 \mathcal{J}_2 \cos[2(\theta_1 - \theta_2)] \}, \end{aligned} \quad (86)$$

and

$$0 \leq \mathcal{J}_1 + \mathcal{J}_2 \leq 1. \quad (87)$$

This is precisely the zero temperature classical Hamiltonian with a coupling strength  $\chi_\beta$ . From the above expression we can conclude that the temperature effect in the SCR is the same as observed for the  $SU(2)$  version of the model [37] and for the Maser model (also chaotic) [11, 12], i.e., the temperature does not bring new dynamical effects. It is, however, important to stress that the thermal states cannot be simulated by simply changing the parameters of the Hamiltonian and are effectively distinct with respect to those corresponding to zero temperature.

### V.2.A. Fixed Points and Bifurcations in the Strong Coupling Regime

The equations of motion for the strong coupling regime obtained from Hamiltonian (78) are given by

$$\dot{\eta}_1 = -\frac{\partial E}{\partial \theta_1} = 2\eta_1\chi\{-(T - \eta_1 - \eta_2)\sin(2\theta_1) + \eta_2\sin[2(\theta_1 - \theta_2)]\}, \quad (88)$$

$$\dot{\eta}_2 = -\frac{\partial E}{\partial \theta_2} = -2\eta_2\chi\{(T - \eta_1 - \eta_2)\sin(2\theta_2) + \eta_1\sin[2(\theta_1 - \theta_2)]\}, \quad (89)$$

$$\begin{aligned} \dot{\theta}_1 = \frac{\partial E}{\partial \eta_1} = & 1 + \chi\{-(T - 2\eta_1 - \eta_2)\cos(2\theta_1) + \eta_2[\cos(2\theta_2) \\ & + \cos[2(\theta_1 - \theta_2)]]\}, \end{aligned} \quad (90)$$

$$\dot{\theta}_2 = \frac{\partial E}{\partial \eta_2} = 2 + \chi\{\eta_1[\cos(2\theta_1) + \cos[2(\theta_1 - \theta_2)]] - (T - \eta_1 - 2\eta_2)\cos(2\theta_2)\}. \quad (91)$$

The variables  $\eta_1$  and  $\eta_2$  are directly connected to the population of the levels. The model has a very rich classical structure which has been previously studied in the zero temperature limit [24]. We have studied thirteen of the fourteen stationary points analytically. In Table II we give the energies, coordinates and validity range of these solutions at finite temperature. In Fig. 14 we display the zero temperature energies as a function of  $\chi$  for attractive and repulsive interactions. It is important to notice the difference on the bifurcations of minima in the two cases. For negative  $\chi$  values we have two bifurcations of equilibrium: for  $-1 \leq \chi \leq 0$  we have one single minimum ( $H$  solution). At  $\chi = -1$ , this bifurcates to two minima ( $K$  solution) and becomes a saddle solution. The  $K$  solution stays that way in the interval  $-3 \leq \chi \leq -1$ . At  $\chi = -3$  four symmetrical minima appear ( $N$  solution) and  $K$  becomes unstable. The positive  $\chi$  value present one minimum for  $\chi < 1$  ( $H$  solution) and only one bifurcation to two minima for  $\chi \geq 1$  ( $A$  solution).

These ground state solutions of the Hamiltonian, as well as their bifurcations are intimately related with the thermodynamical regimes and their phase transitions. Although we have not made the calculations for attractive interactions, we can

TABLE II

Energy, Coordinates  $(\eta_1, \eta_2, \theta_1, \theta_2)$  and Range of Validity as a Function of Coupling Parameter  $\chi$  and Temperature Dependent Term  $T = T_1 = T_2$  of 13 of the 14 Fixed Points of Classical Hamiltonian (78) for Strong Coupling Regime

Point	$E$	$\eta_1$	$\eta_2$	$\theta_1$	$\theta_2$	Validity
A	$\frac{-(\chi T + 1)^2}{4\chi}$	$\frac{\chi T - 1}{2\chi}$	0	0	—	$ \chi T  \geq 1$
B	$\frac{-(\chi^2 T^2 + 4)}{4\chi}$	0	$\frac{\chi T - 2}{2\chi}$	—	0	$ \chi T  \geq 2$
C	$\frac{-(\chi T + 1)^2}{5\chi}$	$\frac{\chi T - 4}{5\chi}$	$\frac{\chi T + 1}{5\chi}$	0	0	$\chi T \leq -1$ or $\chi T \geq 4$
D	$\frac{-(\chi T - 1)^2}{4\chi}$	$\frac{\chi T + 1}{2\chi}$	$\frac{\chi T - 1}{2\chi}$	$\theta_2 + \frac{\pi}{2}$	$\cos(2\theta_2) = \frac{3 - \chi T}{2}$	$1 \leq \chi T \leq 5$
E	$\frac{-(\chi^2 T^2 - 5)}{5\chi}$	$\frac{3T}{5}$	$\frac{\chi T + 5}{5\chi}$	0	$\frac{\pi}{2}$	$ \chi T  \geq 5$
F	$\frac{-(\chi T - 1)^2}{5\chi}$	$\frac{\chi T + 4}{5\chi}$	$\frac{3(\chi T - 1)}{5\chi}$	$\frac{\pi}{2}$	0	$\chi T \leq -4$ or $\chi T \geq 1$
H	$-T$	0	0	—	—	$\forall \chi, T$
I	0	$T$	0	$\cos(2\theta_1) = \frac{-1}{\chi T}$	—	$ \chi T  \geq 1$
J	$+T$	0	$T$	—	$\cos(2\theta_2) = \frac{-2}{\chi T}$	$ \chi T  \geq 2$
K	$\frac{(\chi T - 1)^2}{4\chi}$	$\frac{\chi T + 1}{2\chi}$	0	$\frac{\pi}{2}$	—	$ \chi T  \geq 1$
L	$\frac{\chi^2 T^2 + 4}{4\chi}$	0	$\frac{\chi T + 2}{2\chi}$	—	$\frac{\pi}{2}$	$ \chi T  \geq 2$
M	$\frac{(\chi T + 1)^2}{4\chi}$	$\frac{\chi T - 1}{2\chi}$	$\frac{\chi T + 1}{2\chi}$	$\cos(2\theta_1) = \frac{-(\chi T + 3)}{2\chi T}$	$\theta_1$	$\chi T \leq -1$ or $\chi T \geq 3$
N	$\frac{\chi^2 T^2 + 3}{3\chi}$	$\frac{T}{3}$	$\frac{\chi T + 3}{3\chi}$	$\frac{\pi}{2}$	$\frac{\pi}{2}$	$ \chi T  \geq 3$

*Note.* The fixed points are labeled from A to N. The point G can be found numerically and is omitted here.

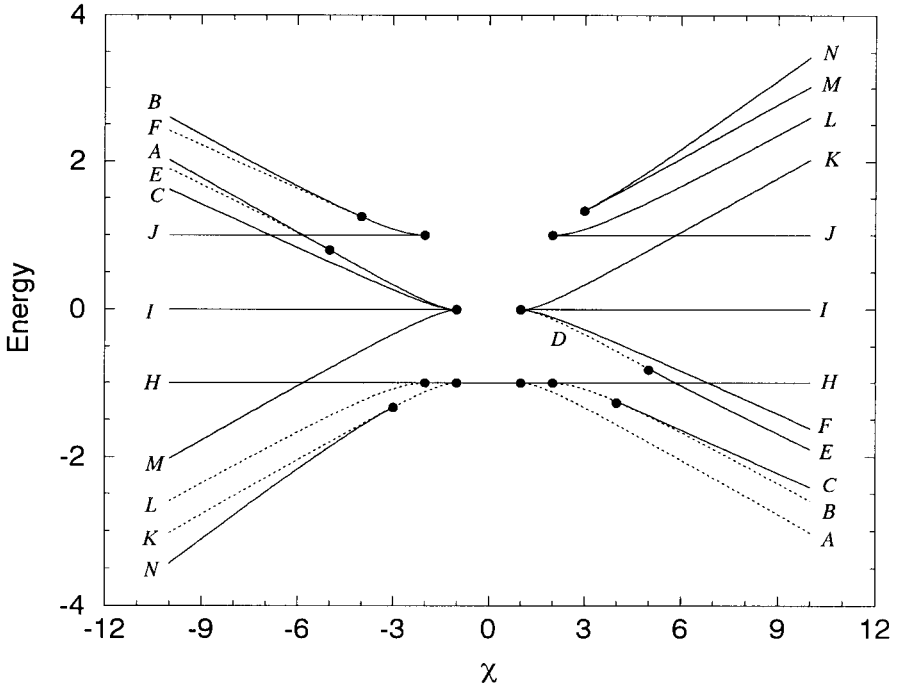


Fig. 14. Classical energy of stationary points as function of coupling parameter  $\chi$  at zero temperature. These points are labeled from  $A$  to  $N$ . The point  $G$  can just be found numerically and it is omitted here. The black circles indicate the bifurcations and the dotted lines are used to detach the solutions. For attractive interaction there are three minimum solutions ( $N$  (four minima),  $K$  (two minima) and  $H$  (one minimum)). For repulsive interaction there are just two minimum solutions ( $A$  (two minima) and  $H$  (one minimum)). The ground state energy phase transitions are related with the thermodynamical phase transitions.

expect to find just one phase transition and two thermodynamical phases. The respective phase to strong coupling regime does not exist in this situation.

### V.3. Large Amplitude Motion for All Regimes

In this section we study the thermal classical dynamics in the context of the Heisenberg equations of motion [41] for the average values of the Lie algebra generators  $G_{jk}$ , i.e.,

$$i \frac{d}{dt} \text{Tr}(DUG_{jk} U^\dagger) = \text{Tr}(DU[G_{jk}, H] U^\dagger), \quad (92)$$

where  $j, k = 0, 1, 2$ ,  $H$  is given by (17) and  $G_{jk}$  are the nine generators of  $U(3)$  algebra which obey the commutation relations (16) and conserve the quantities

$$C_1 = \sum_i G_{ii} = N, \quad (93)$$

$$C_2 = \sum_{i,j} G_{ij} G_{ji}, \quad (94)$$

$$C_3 = \sum_{i,j,k} G_{ij} G_{jk} G_{ki}. \quad (95)$$

The conservation of  $C_1$  restricts the  $U(3)$  algebra to the  $SU(3)$ , whose Casimir operators are  $C_2$  and  $C_3$ .  $U$  and  $D$  have the same form as presented in the previous section. We will take the large  $N$  limit of these equations of motion. Thus the classical dynamics of the system is governed by nine differential equations which are not completely independent, due to the above conservation equations, besides the total energy of the system. The classical variables now correspond to the classical limit of the average values of the generators of the algebra. The dynamical equations in the large  $N$  limit are

$$i\dot{X}_{01} = X_{01} + \chi((I_0 - I_1) X_{10} - X_{20} X_{21} + X_{12} X_{02}), \quad (96)$$

$$i\dot{X}_{10} = -X_{10} + \chi((I_1 - I_0) X_{01} + X_{02} X_{12} - X_{21} X_{20}), \quad (97)$$

$$i\dot{X}_{02} = 2X_{02} + \chi((I_0 - I_2) X_{20} - X_{10} X_{12} + X_{21} X_{01}), \quad (98)$$

$$i\dot{X}_{20} = -2X_{20} + \chi((I_2 - I_0) X_{02} - X_{12} X_{10} + X_{01} X_{21}), \quad (99)$$

$$i\dot{X}_{12} = X_{12} + \chi((I_1 - I_2) X_{21} - X_{01} X_{02} + X_{10} X_{20}), \quad (100)$$

$$i\dot{X}_{21} = -X_{21} + \chi((I_2 - I_1) X_{12} - X_{02} X_{01} + X_{10} X_{20}), \quad (101)$$

$$i\dot{I}_0 = \chi(X_{01}^2 - X_{10}^2 + X_{02}^2 - X_{20}^2), \quad (102)$$

$$i\dot{I}_1 = \chi(X_{10}^2 - X_{01}^2 + X_{12}^2 - X_{21}^2), \quad (103)$$

$$i\dot{I}_2 = \chi(X_{20}^2 - X_{02}^2 + X_{21}^2 - X_{12}^2). \quad (104)$$

In the classical limit (where fluctuation corrections of order of  $1/N$  are neglected) we have

$$X_{01} = \frac{1}{N} \text{Tr}(DUG_{01}U^\dagger) = -iz_1 \frac{S_1 C_1}{R_1} \{T_1 + S_3^2 T_3 - S_2^2 (T_2 - S_3^2 T_3)\} \\ - \left\{ z_2 z_3^* \frac{C_1^2 S_2 S_3 C_3}{R_2 R_3} + \frac{z_1 z_2^* z_3}{z_1^*} \frac{S_1^2 S_2 S_3 C_3}{R_2 R_3} \right\} T_3, \quad (105)$$

$$X_{02} = \frac{1}{N} \text{Tr}(DUG_{02}U^\dagger) = -iz_2 \frac{C_1 S_2 C_2}{R_2} (T_2 - S_3^2 T_3) + z_1 z_3 \frac{S_1 C_2 S_3 C_3}{R_1 R_3} T_3, \quad (106)$$

$$X_{12} = \frac{1}{N} \text{Tr}(DUG_{12}U^\dagger) = -iz_3 \frac{C_1 C_2 S_3 C_3}{R_3} T_3 + z_1^* z_2 \frac{S_1 S_2 C_2}{R_1 R_2} (T_2 - S_3^2 T_3), \quad (107)$$

$$X_{10} = X_{01}^*, \quad X_{20} = X_{02}^*, \quad X_{21} = X_{12}^*, \quad (108)$$

$$I_0 = \frac{1}{N} \text{Tr}(DUG_{00} U^\dagger) = \text{Tr}(DG_{00}) - S_2^2(T_2 - S_3^2 T_3) - S_1^2[T_1 + S_3^2 T_3 - S_2^2(T_2 - S_3^2 T_3)] - i(z_1 z_2^* z_3 - z_1^* z_2 z_3^*) \frac{S_1 C_1 S_2 S_3 C_3}{R_1 R_2 R_3} T_3, \quad (109)$$

$$I_1 = \frac{1}{N} \text{Tr}(DUG_{11} U^\dagger) = \text{Tr}(DG_{11}) - S_3^2 T_3 + S_1^2[T_1 + S_3^2 T_3 - S_2^2(T_2 - S_3^2 T_3)] + i(z_1 z_2^* z_3 - z_1^* z_2 z_3^*) \frac{S_1 C_1 S_2 S_3 C_3}{R_1 R_2 R_3} T_3, \quad (110)$$

$$I_2 = \frac{1}{N} \text{Tr}(DUG_{22} U^\dagger) = \text{Tr}(DG_{22}) + S_3^2 T_3 + S_2^2(T_2 - S_3^2 T_3), \quad (111)$$

where the terms  $S_j$ ,  $C_j$ ,  $R_j$  and  $T_j$  are the same defined before (60). Note that  $I_k$  is the average value of the number of particles in level  $k$  and  $I_0 + I_1 + I_2 = 1$ . We found it convenient to define the following new variables

$$X_{01} = S_\alpha + iA_\alpha, \quad (112)$$

$$X_{02} = S_\beta + iA_\beta, \quad (113)$$

$$X_{12} = S_\gamma + iA_\gamma, \quad (114)$$

where  $S_\alpha, A_\alpha, S_\beta, A_\beta, S_\gamma, A_\gamma \in \mathbb{R}$ . In terms of these variables the system's Hamiltonian is given by

$$\mathcal{H} = \frac{H}{N} = I_2 - I_0 + \frac{\chi}{2} \{S_\alpha^2 - A_\alpha^2 + S_\beta^2 - A_\beta^2 + S_\gamma^2 - A_\gamma^2\}, \quad (115)$$

and the equations of motion become

$$i\dot{I}_0 = 4\chi(S_\alpha A_\alpha + S_\beta A_\beta), \quad (116)$$

$$i\dot{I}_1 = 4\chi(-S_\alpha A_\alpha + S_\gamma A_\gamma), \quad (117)$$

$$i\dot{I}_2 = -4\chi(S_\beta A_\beta + S_\gamma A_\gamma), \quad (118)$$

$$i\dot{S}_\alpha = A_\alpha + \chi\{-A_\alpha(I_0 - I_1) + 2(A_\beta S_\gamma + S_\beta A_\gamma)\}, \quad (119)$$

$$i\dot{A}_\alpha = -S_\alpha\{1 + \chi(I_0 - I_1)\}, \quad (120)$$

$$i\dot{S}_\beta = 2A_\beta + \chi\{-A_\beta(I_0 - I_2) + 2(A_\alpha S_\gamma - S_\alpha A_\gamma)\}, \quad (121)$$

$$i\dot{A}_\beta = -S_\beta\{2 + \chi(I_0 - I_2)\}, \quad (122)$$

$$i\dot{S}_\gamma = A_\gamma + \chi\{-A_\gamma(I_1 - I_2) - 2(A_\beta S_\alpha + S_\beta A_\alpha)\}, \quad (123)$$

$$i\dot{A}_\gamma = -S_\gamma\{1 + \chi(I_1 - I_2)\}. \quad (124)$$

This is the system of equations which we will study in order to understand the influence of thermal effects on the chaotic portion of phase space. Before proceeding, however, it is important to analyse the new classical variables which describe the system. As already mentioned, the third degree of freedom does not bring novel interpretations to the variables  $I_k$ , since they stay the same as before: they are the classical analogue of the occupation number of each of the three shells and obey a constraint equation. They also stand for the action variables of the free system. However the variables which are the classical analogue to the transition operators require a more careful analysis. They are conveniently expressed as

$$X_{01} = \langle G_{01} \rangle = \rho_\alpha e^{i\theta_\alpha}, \quad (125)$$

$$X_{02} = \langle G_{02} \rangle = \rho_\beta e^{i\theta_\beta}, \quad (126)$$

$$X_{12} = \langle G_{12} \rangle = \rho_\gamma e^{i\theta_\gamma}. \quad (127)$$

In particular for zero temperature and the SCR (when  $T_3 = 0$ ) they acquire the form

$$X_{01} = \sqrt{I_0 I_1} e^{i\theta_1}, \quad (128)$$

$$X_{02} = \sqrt{I_0 I_2} e^{i\theta_2}, \quad (129)$$

$$X_{12} = \sqrt{I_1 I_2} e^{i(\theta_1 - \theta_2)}, \quad (130)$$

that is, the modulus of these variables are action-type variables. Thus, for example, we have that  $\rho_\alpha$  is expressed in terms of  $I_0$  and  $I_1$ , implying in fact that from the variables  $X_{01}$  and  $X_{10}$  we only get information about *one* independent classical variable and not two as can be expected in the general case. This independent variable is precisely the variable  $\theta_1$ , canonically conjugate to  $I_1$ . A similar situation occurs with  $X_{02}$  and  $X_{20}$ . On the other hand  $X_{12}$  and  $X_{21}$  present a remarkable behavior: besides their modulus, their phase is also a function of well known classical variables. Schematically we have

$$\begin{array}{ccc}
 \left. \begin{array}{l} I_0 \\ I_1 \\ I_2 \end{array} \right\} & \xRightarrow{c_1} & \left\{ \begin{array}{l} I_1 \\ I_2 \end{array} \right. \\
 \left. \begin{array}{l} X_{01} \\ X_{10} \end{array} \right\} & \xRightarrow{\quad} & \theta_1 \\
 \left. \begin{array}{l} X_{02} \\ X_{20} \end{array} \right\} & \xRightarrow{\quad} & \theta_2 \\
 \left. \begin{array}{l} X_{12} \\ X_{21} \end{array} \right\} & \xRightarrow{\quad} & \emptyset \\
 \text{Average values of the} & \xRightarrow{\quad} & \text{Independent classical} \\
 \text{algebra generators} & & \text{variables}
 \end{array}$$

We thus conclude that the classical dynamics of the  $SU(3)$  Lipkin model, at zero temperature or in the SCR, besides the reduction from 9 to 6 variables, suffers a further reduction from 6 to 4 due to the particular interrelation between  $X_{12}$ ,  $X_{01}$ ,  $X_{02}$ ,  $I_0$ ,  $I_1$  and  $I_2$ .

Now, for the other regimes, this last reduction is not possible and Eqs. (128) to (130) are no longer satisfied. Besides numerous trials in analytical form in order to find relations between  $\{\rho_j\}$  and  $\{I_j\}$ , numerical investigation has been implemented in the following way: while integrating the orbits in the ICR some quantities have been controlled as e.g.  $X_{01}X_{10}/(I_0I_1)$ . In the SCR this quantity is equal to unity. However, for the ICR it is a strongly dependent function of time. In the same way we have observed the quantity  $\theta_\gamma - (\theta_\alpha - \theta_\beta)$  and found (instead of zero for SCR) the same dynamical pattern.

### V.3.A. Numerical Procedure and Results

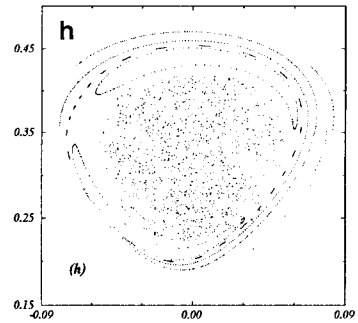
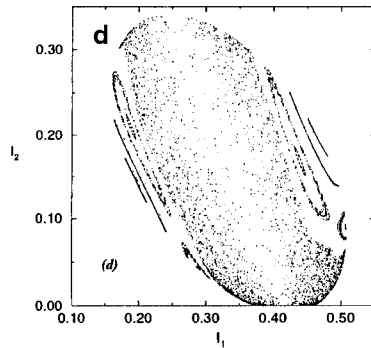
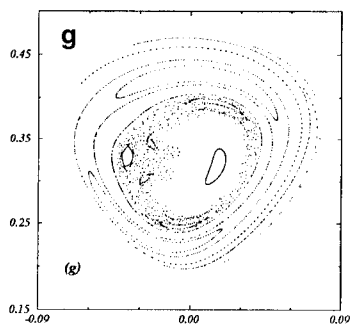
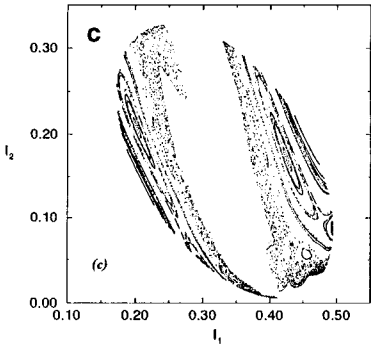
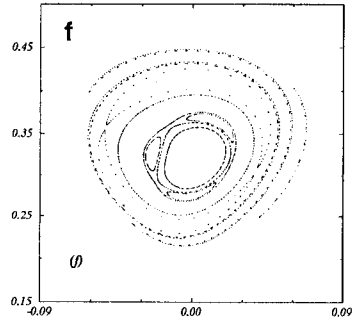
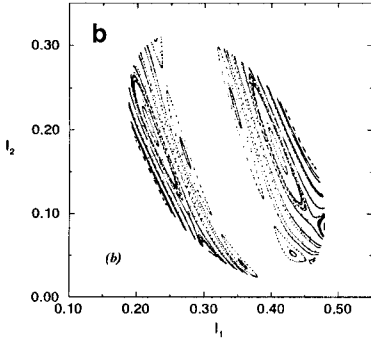
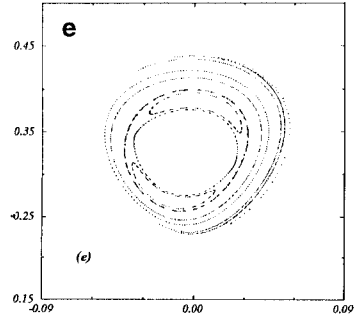
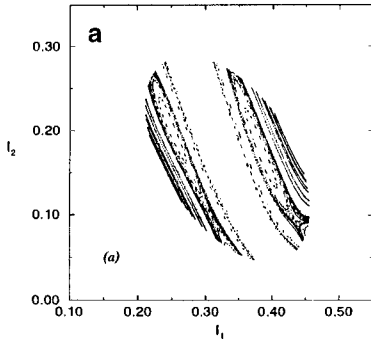
We have used a FORTRAN routine of the Numerical Recipes Library which uses a fifth order Runge Kutta integration method to integrate our equations. The total energy, coupling constant and the parameters  $T_1$  and  $T_2$  are given. The initial complex variables  $z_1$ ,  $z_2$  and  $z_3$  are randomly generated. Given the set  $\{z_k\}$  the dynamical variables are calculated from (105)–(111) and the trajectory is obtained after integrating (116)–(124). It is important to remark that the motion with three degrees of freedom occurs on a submanifold of dimension 5 due to the conservations (93)–(95) and energy. In practice we have eliminated only one dimension by using (93) and integrated a set of eight coupled equations. Since the system has more than two degrees of freedom, we will have a hamiltonian flux with characteristics which are radically new with respect to the two degree of freedom case. These novel features have been the subject of investigation in the literature [1, 4, 6]. We quote two of them: for a two-degrees of freedom system the bidimensional KAM surfaces divide the tridimensional “volume” of the same energy in phase space in a set of closed volumes, each one of them involved and limited by KAM surfaces. For three degrees of freedom the tridimensional KAM surfaces do not divide the 5-dimensional energy volume in a set of closed volumes. For  $n > 2$ ,  $n$  being the number of degrees of freedom, the KAM surfaces do not divide the energy volume of  $(2n - 1)$  dimensions in distinct regions. So we have that, in this case all the stochastic shells of the energy surface in phase space are connected in a complex net called Arnold’s web. This web is spread in all phase space, either by intercepting or by being infinitesimally close to all points. This motion is known as Arnold diffusion [42, 43]. We can note, however, that this process is far too slow in comparison to the diffusion of the trajectory within its original stochastic shell. The second novel aspect of the dynamics is the fact that energy conservation does not avoid large stochastic motion along the shells anymore for large enough times. Although we are not particularly interested in investigating these aspects, it is important to have them in mind and take their implications into account.

In what follows we present two methods which we have used to study the three degrees of freedom dynamics. One of them is of qualitative character and the other quantitative. The first one consists of a well known graphical method. Since the Poincaré sections will have four dimensions, as we will shortly see, some alternative graphical representations have been adopted, allowing for a comparison between the trajectories of the system at zero temperature with the ICR and WCR trajectories. The second method consists in the calculation of the largest Lyapunov exponent of the dynamics and of the chaotic volume of the system, i.e., the phase space volume in which at least one Lyapunov exponent is positive. This analysis allows for the characterization of the finite temperature effects on the dynamics by means of a quantitative and definite criterion.

*Graphical method: “Poincaré sections.”* The concept of Poincaré section or surface of section can be generalized for systems with  $n > 2$ . For the usual case,  $n = 2$ , among the four phase space coordinates (related through energy conservation), one chooses one of them, defining thus the surface. One then considers the successive trajectory intersections with this section which satisfy another condition: that one of the left out coordinates possesses values within a restricted predetermined interval so that the Poincaré map may be defined as a diffeomorphism. Given that this condition is satisfied, the restricted coordinate of the intersection point of the trajectory with the section is ignored. This is equivalent to a “partial projection” of the trajectory onto this coordinate. The other pair of coordinates is then collected defining thus a set of points. They can be on a manifold of dimension one, in the case there is at least one constant of motion besides the energy, or on a manifold of dimension up to two, in the case there is no such conservation. For  $n > 2$  the surface of section is defined as a manifold of  $(2n - 2)$  dimensions and one considers the successive intersections of the trajectory with this surface. Thus, in our case the Poincaré sections have four dimensions, the set of points of which can be on manifolds from 2 to 4 dimensions.

Other authors have also faced this problem. In ref. [6] there are two citations of the work of C. Froeschlé [44, 45] as being one of the few pioneers with the courage to attack this problem. In [44] two graphical methods are described and tested in a particular case. They are: slice cutting and stereoscopic views. However, they have not been useful to us. Particularly the first one require a very long time and high precision computation in order to get a few quantity of points in the sections. So we have made the option for two types of graphical representations of the Poincaré sections of our dynamics that made possible the comparison between the known two degrees of freedom dynamics (SCR and zero temperature) and the new three degrees of freedom motion (ICR and WCR). They are as follows:

1. We plot  $I_1 \times I_2$  when the trajectory goes through  $A_\alpha = 0$  and  $S_\alpha > 0$  (these conditions define the section),  $S_\beta > 0$  and  $A_\beta > 0$  (a necessary condition for the map to be a diffeomorphism). For the SCR these conditions imply  $\theta_1 = 0$  and  $0 < \theta_2 < \pi/2$ , where  $\theta_1$  and  $\theta_2$  are angle type variables as defined by (76).



2. We plot  $I_1 \cos(\theta) \times I_1 \sin(\theta)$  when the trajectory crosses fixed  $I_2$ ,  $S_\beta > 0$  and  $A_\beta > 0$ , where

$$\cos(\theta) \equiv \frac{S_\alpha}{\sqrt{S_\alpha^2 + A_\alpha^2}}, \quad (131)$$

i.e., the real part of  $\langle G_{01} \rangle$  divided by its norm and

$$\sin(\theta) \equiv \frac{A_\alpha}{\sqrt{S_\alpha^2 + A_\alpha^2}}, \quad (132)$$

its imaginary part, divided by its norm.

In the case  $T_3 = 0$  (SCR) the variable  $\theta$  is precisely the variable which is canonically conjugate to  $I_1$ . Now, the representations of item (1) for  $T_3 = 0$  are equivalent to sections in the  $\theta_1 = 0$  plane. It is important to emphasize that item (1) is just valid for  $\chi \neq 0$ , since the hamiltonian flux can not be tangent to the section.

Our results are the following (note the difference in the scales of the several figures): in Fig. 15 we present the sections  $I_1 \times I_2$  (left column) and  $I_1 \cos(\theta) \times I_1 \sin(\theta)$  (right column) for  $\chi = -6$  and zero temperature and increasing energies (a, e)  $E = -2.10$ , (b, f)  $E = -2.07$ , (c, g)  $E = -2.05$  and (d, h)  $E = -2.03$ . These energies are close to those of the point  $N$ , the minimum  $E_{min} = -2.1666$  ( $\chi = -6.0$ ). We observe the regular character of the trajectories close to the minimum and the increase of chaos as the energy grows. The finite temperature analysis of the two kinds of plots lead to the same conclusions, so we restrict ourselves to presenting the item (2) results.

In Fig. 16 we show  $(I_1, \theta)$  for  $\chi = -2$ , zero temperature and increasing energies. These trajectories are close to the point  $K$  ( $E_{min} = -1.125$ ) which is a minimum for  $-3 < \chi < -1$ . Note that at an energy value 11% larger than the minimum, the orbits are still regular (see Fig. 16(c)). The section is defined for  $I_2 = 0.001$  in (a) and (b) and  $I_2 = 0.05$  in (c) and (d).

In Fig. 17 we maintain  $\chi = -2$  and take  $\beta = 1.62$ . These parameter values correspond to the ICR. It is worth pointing out that for this  $\chi$  value the phase SCR does not exist and  $T_3$  is no longer zero. The trajectories of these figures have energies (a)  $E = -0.97$ , (b)  $E = -0.90$  and (c)  $E = -0.85$ . The value of the minimum energy, i.e., of the point  $K$  is now  $-0.9732$ . These plots show radical differences with respect to the previous one: at an energy around 0.33% larger than the minimum energy the orbits *apparently* loose their regularity. We can also observe the

---

Fig. 15. Poincaré sections  $I_1 \times I_2$  (left column) and  $I_1 \cos(\theta) \times I_1 \sin(\theta)$  through the plane  $\eta_2 = 0.166$  (right column) for several trajectories at zero temperature (where  $\theta = \theta_1$ ) and  $\chi = -6.0$  near the minimum point (solution  $N$ ) for increasing energies (a, e)  $E = -2.10$ , (b, f)  $E = -2.07$ , (c, g)  $E = -2.05$  and (d, h)  $E = -2.03$ . The minimum energy is  $-2.1666$ . In the right column sections, we show only the upper hemisphere ( $0 \leq \theta \leq \pi$ ).

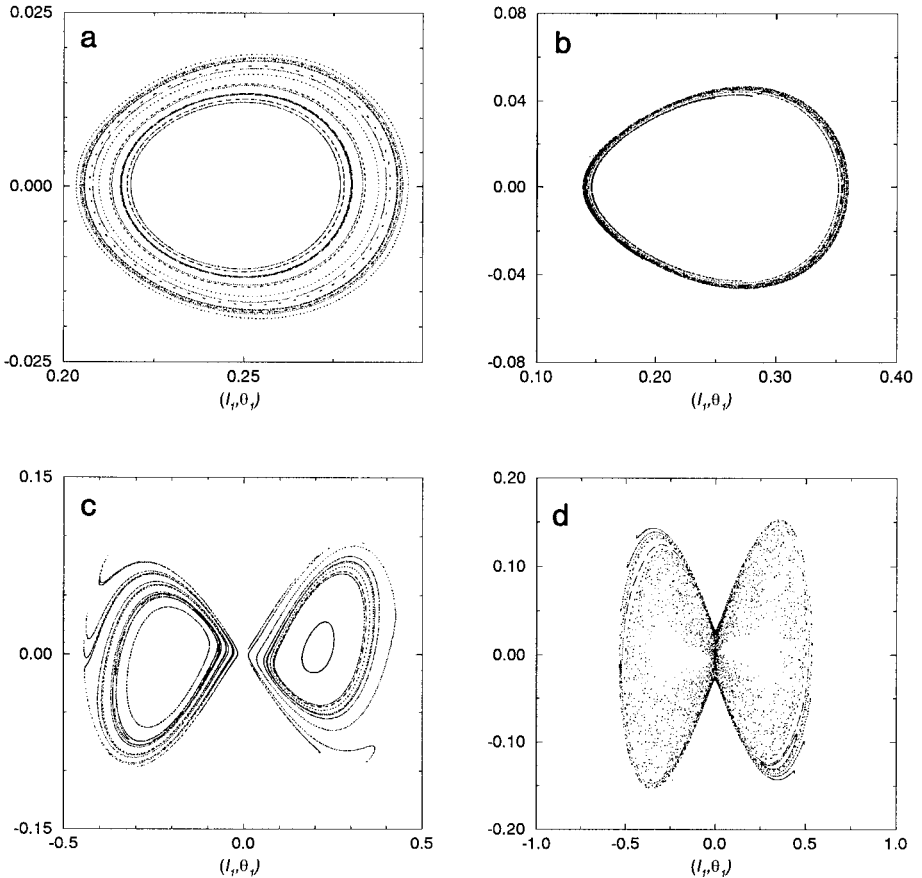


Fig. 16. Graphical representations of *type (2)* for several trajectories near the minimum point  $K$  at zero temperature,  $\chi = -2.0$  and increasing energies (a)  $E = -1.12$ , (b)  $E = -1.10$ , (c)  $E = -1.00$  and (d)  $E = -0.90$ . The sections are defined by fixed  $I_2$  equal to 0.001 at (a) and (b) and 0.050 at (c) and (d).

appearance of a new structure close to  $\Theta = \pm\pi/2$  in Fig. 17(c) which is not present at 16(d), its corresponding one at zero temperature.

For a larger temperature value  $\beta = 1.2$ , which is very close to the  $ICR \rightarrow WCR$  phase transition, we note that the system shows an even more distinct behavior. For these parameters values,  $E_{min} = -0.6584$ . In Fig. 18 we show graphic representations of the trajectories for (a)  $E = -0.655$  with  $I_2 = 0.067$  and (b)  $E = -0.60$  with  $I_2 = 0.08$ . Note that even for orbits very close to  $E_{min}$ , the variable  $\Theta$  (now *not* canonically conjugate to  $I_1$ ) strongly varies throughout to  $[0, 2\pi]$  interval.

The above results allow us to conclude that:

1. The temperature effect on the classical dynamics in the ICR and WCR is really far from being a scaling since the patterns observed for the trajectories is completely distinct from those at zero temperature.

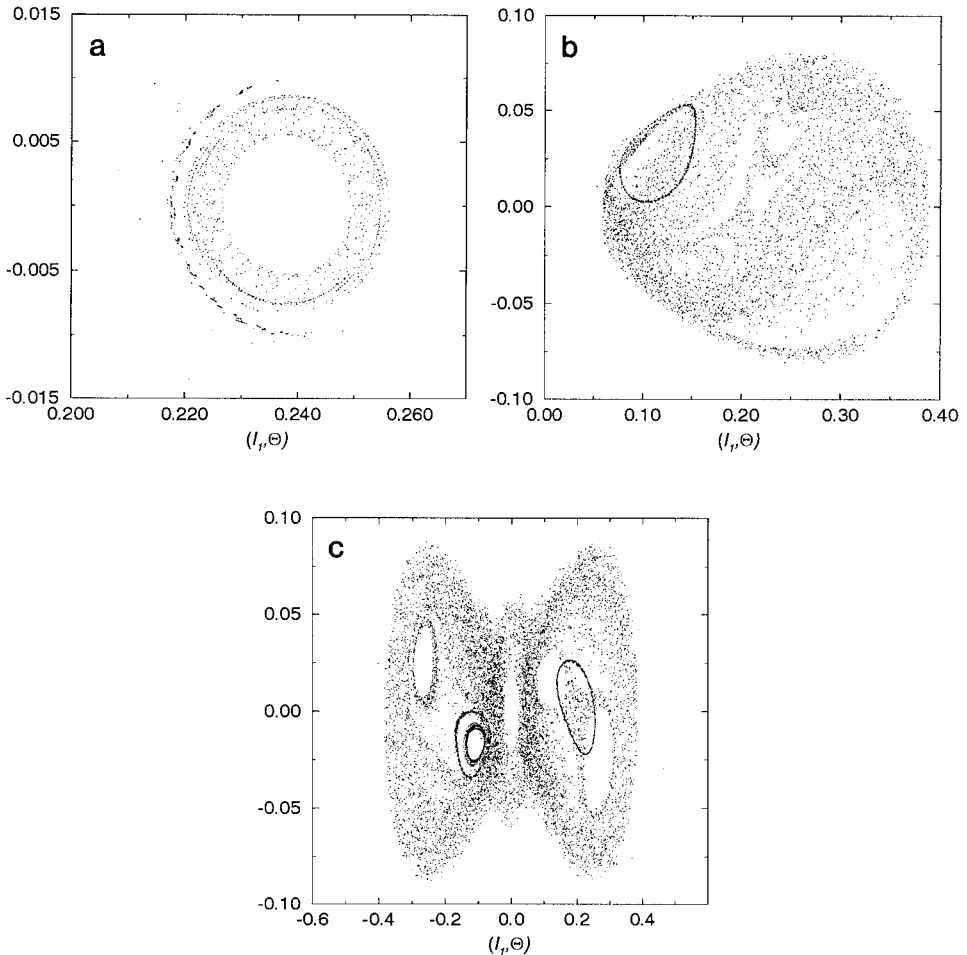


Fig. 17. Graphical representation of *type (2)* for several trajectories near the minimum point  $K$  at *finite temperature*  $\beta = 1.62$ ,  $\chi = -2.0$  and increasing energies (a)  $E = -0.97$ , (b)  $E = -0.90$  and (c)  $E = -0.85$ . The sections are defined by fixed  $I_2$  equal to (a) 0.024, (b) 0.050 and (c) 0.100. The minimum energy for these parameters is  $-0.9732$  and  $T_3 = 0.0353$ .

2. A third degree of freedom is really active in these two phases. Should there be some other conservation law in the system besides energy, this would be reflected in the plots.

3. The presented graphical representations are absolutely inadequate for the purpose of qualifying the system as regular or chaotic. The Lyapunov's exponents analysis, presented in what follows, shows, on one hand that patterns which seen highly chaotic in the above representations may correspond to trajectories with zero

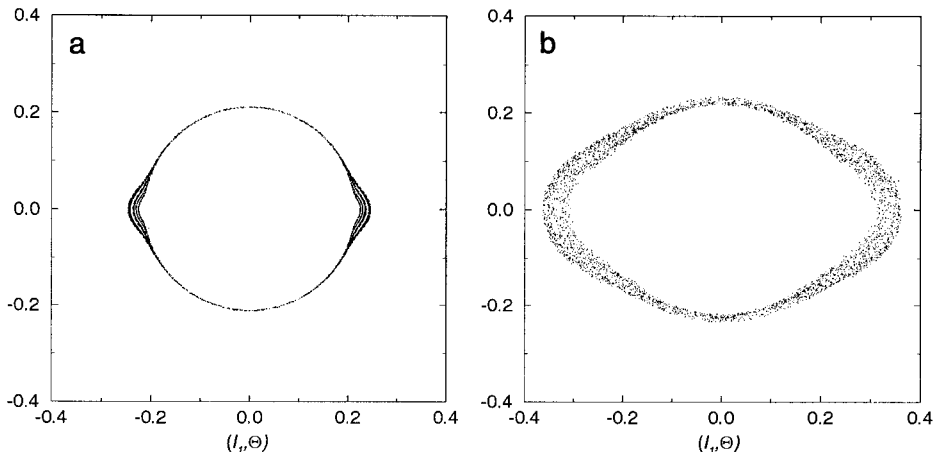


Fig. 18. The same as the last figure for *finite temperature*  $\beta = 1.2$ ,  $\chi = -2$  and increasing energies (a)  $E = -0.655$  and  $I_2^{\text{fixed}} = 0.067$  and (b)  $E = -0.60$  and  $I_2^{\text{fixed}} = 0.08$ . This temperature is near the  $\text{ICR} \rightarrow \text{WCR}$  phase transition.  $E_{\text{min}} = -0.6584$  and  $T_3 = 0.1474$ .

Lyapunov exponents, and on the other hand, seemingly regular curves may have positive Lyapunov exponent.

*Quantitative method: Lyapunov exponents and the chaotic volume.* We now apply the same procedure as in ref. [23] in the study of the zero temperature case, in order to quantitatively characterize the thermal dynamical effects in the ICR and WCR.

Given a particular trajectory with initial condition  $\vec{x}_0$ , we consider a neighbouring trajectory distant from the first one by  $|d_0|$ . We then integrate both trajectories, monitoring them in time intervals  $\tau$  following the numerical procedure established in [46] to calculate the Lyapunov exponent. It is defined as

$$\lambda(\vec{x}_0, t) \equiv \lim_{t \rightarrow \infty} \frac{1}{t} \ln \frac{|d(t)|}{|d_0|}. \quad (133)$$

We are interested in calculating the largest exponent, since it is enough that one of them is positive to characterize the trajectory as chaotic.

In the present investigation, we fix  $\chi$  and  $\beta$  and vary the system's energy. We then calculate the chaotic volume, i.e., the fraction of the accessible phase space in which the Lyapunov's exponent is positive. In practice we divide the complete range of accessible energy values for  $\chi$  and  $\beta$  in bins, adopting variable intervals according to the energy region. For regions of intermediate energy the bins are larger and get smaller at the ends of the energy interval where there is a more rapid variation in the system's behavior. For each one of these bins we randomly choose one hundred initial conditions with energies belonging to the respective energy interval. We

next calculate the Lyapunov's exponents of these trajectories, defining how many, among those, correspond to positive largest exponent and how many to exponent zero. This decision was made by visually observing the  $\lambda(t)$  behavior in log-log scale for each one of the trajectories. The typical zero exponent decreases as  $1/t$ , while the positive becomes constant after some time.

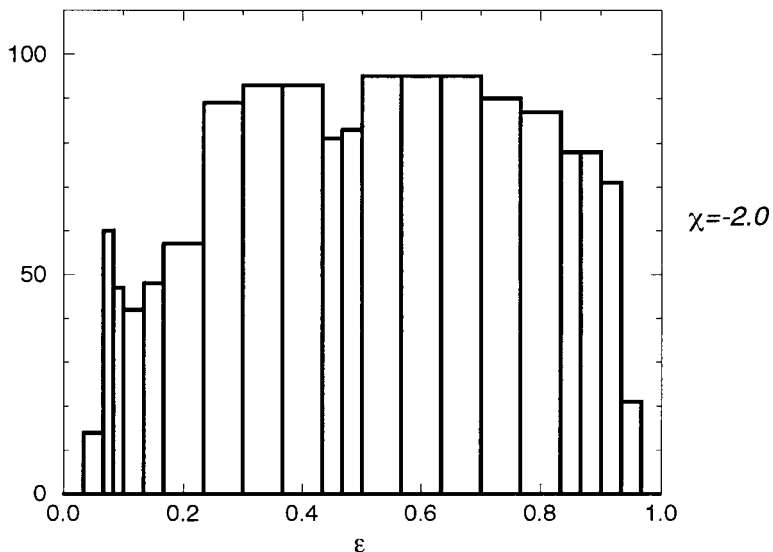
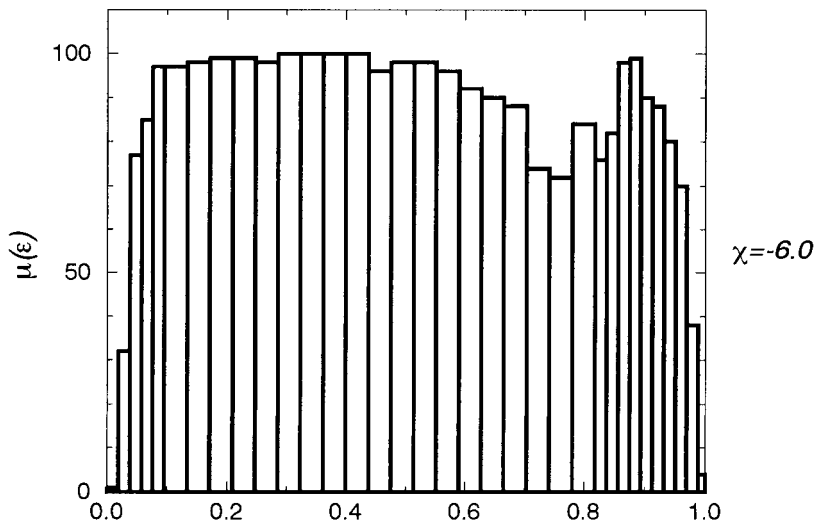


Fig. 19. Chaotic volume of the system as function of renormalized energy for zero temperature for  $\chi = -6.0$  and  $\chi = -2.0$ .

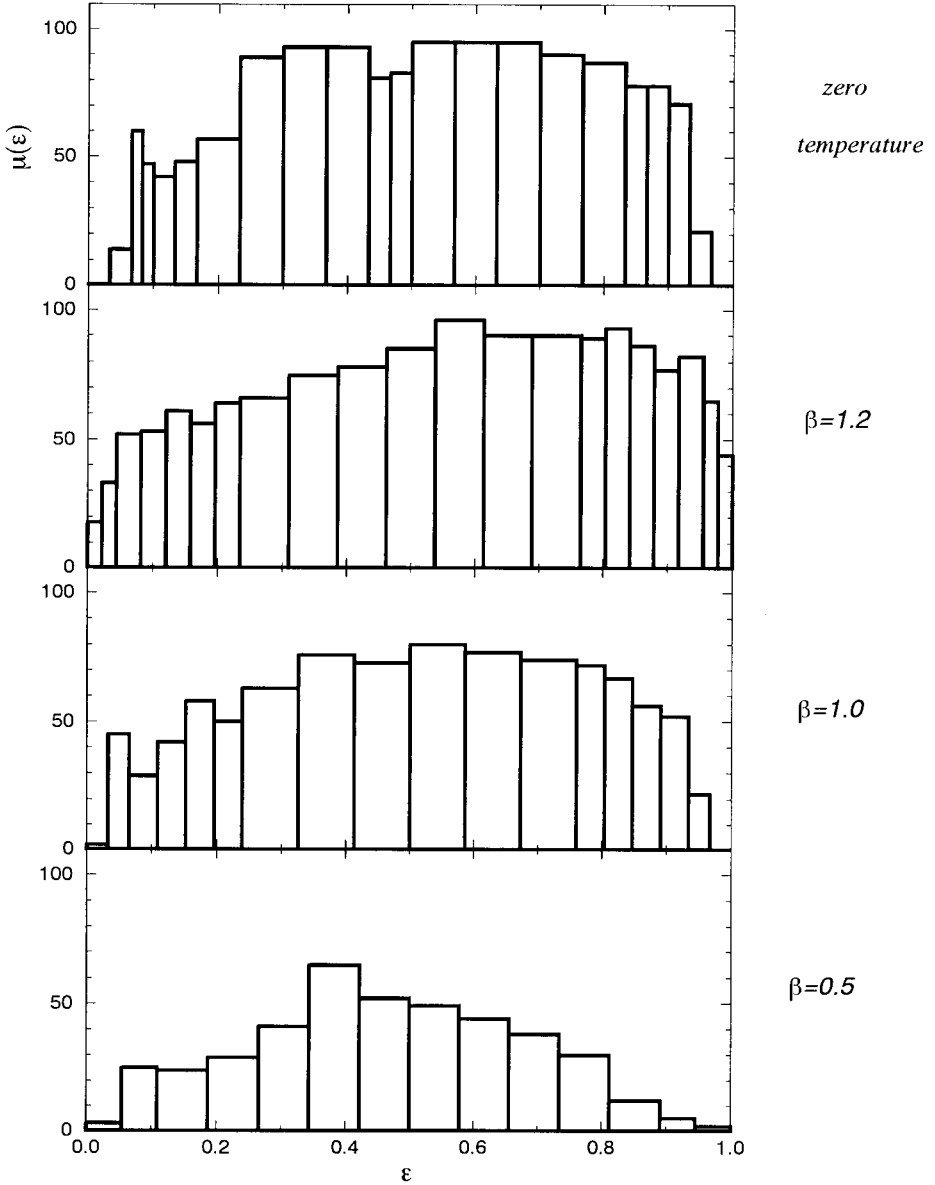


Fig. 20. Chaotic volume of the system as function of renormalized energy for  $\chi = -2.0$  and four different temperatures: zero,  $\beta = -1.2$  (ICR),  $\beta = -1.0$  (WCR) and  $\beta = -0.5$  (WCR).

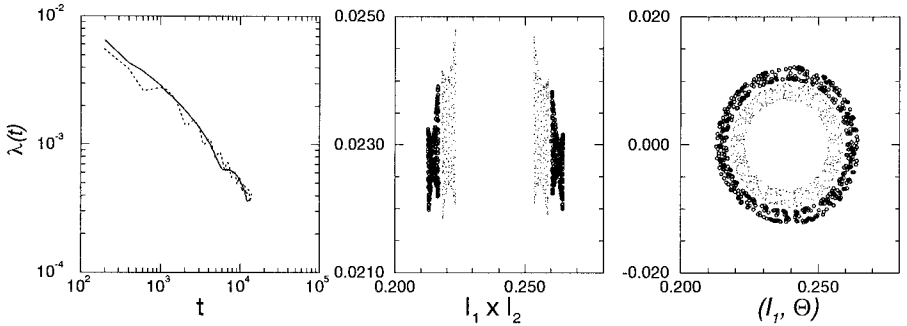


Fig. 21. Graphical representations of type (1) and (2) and the largest Lyapunov exponent as function of time of two different trajectories. One of them is represented by solid line and circles and the other by dashed line and dots. Note that in both cases the exponents diminish with time as a typical zero exponent (regular trajectory) while the graphical representations show irregular patterns.

The results are the following: for zero temperature, we have calculated the chaotic volume as a function of the system's energy for  $\chi = -6.0$  and  $\chi = -2.0$ . This is shown in Fig. 19. The energy spectrum was divided in 34 bins for  $\chi = -6$  and in 22 for  $\chi = -2$ . The energy intervals of the system have been scaled to the interval  $[0, 1]$  to facilitate comparison. We verify that the chaotic volume for  $\chi = -2$  is smaller than for  $\chi = -6$  specially at the ends of the spectrum.

For convenience, in our analysis we adopted  $\chi = -2$ , a value for which the SCR does not exist. The calculation of the chaotic volume was performed for four temperatures (a) zero temperature, (b)  $\beta = 1.2$  (ICR, near the phase transition), (c)  $\beta = 1.0$  (WCR, maximum absolute value of  $T_3$ ) and (d)  $\beta = 0.5$  (WCR). These have been so chosen as to make the thermal effects more conspicuous.

In Fig. 20 we observe that systematically, the chaotic volume of the system decreases with temperature in both phases, affecting most the extremes of the spectrum. This leads us to the conclusion that increasing the temperature tends to counterbalance the dynamical coupling effects. The several novel nonlinear terms in the Hamiltonian do not cause an enhancement of the chaotic volume, as one might naively expect.

For illustration we present Fig. 21 where the graphical representations of type (1) and (2) and the largest Lyapunov exponent are compared for two trajectories. In both cases, trajectories with a chaotic graphical pattern are presented. Both trajectories possess typically zero Lyapunov's exponents. In this way we can safely conclude that the adopted graphical representations are *not* adequate to characterize the chaoticity degree of the trajectories. This is to be expected since we are projecting 4-dimensional sections in two dimensions.

## VI. CONCLUSIONS

We have presented a detailed investigation of the finite temperature effects in the  $SU(3)$  Lipkin model. The thermodynamical analysis reveals that the system can

exhibit three distinct phases as function of the interaction strength and inverse temperature and two second order phase transitions.

A generalized classical limit of the model that incorporates statistical mixtures is derived. We have explicitly shown that one remarkable effect of the temperature in this classical dynamics is giving rise to a new degree of freedom “frozen” in the zero temperature limit. In one of the three regimes, the strong coupling regime, the dynamics has two degrees of freedom. We were able to find two pairs of canonically conjugate variables and to show that the net temperature effect in this phase is just to produce a scaling of the zero temperature dynamics like in the Maser model [11, 12] and in the  $SU(2)$  version of Lipkin model [37]. But in the other two regimes any scaling is really absent and the classical motion present a richer behavior, occurring in a 5-dimension manifold. A quantitative characterization by Lyapunov exponent and chaotic volume of the system lead us to conclude that increasing the temperature tends to counterbalance the dynamical coupling effects. Investigation about the nature and origin of the third degree of freedom is presently under way.

With the present finite temperature study we have shown that:

(i) Temperature restores the symmetry of the system, in this particular case, the parity symmetry. This manifestation is present in other branches of physics such as the restoration of chiral symmetry in QCD effective models.

(ii) Temperature gives rise to a new normal mode. This can be explained by the fact that temperature changes occupation numbers so that highly excited states are mixtures of multi-particle multi-hole states when referred to the ground state. The appearance of this new degree of freedom shows itself in the classical motion of the system by the appearance of trajectories with patterns completely distinct from those at zero temperature.

(iii) The third degree of freedom is a manifestation of the presence of the non-symmetrical representations, i.e. of the Pauli principle. Its full understanding requires the study of the system when its motion is restricted to a single non-symmetrical representation. In particular it would be interesting to study the classical limit ( $N \rightarrow \infty$ ) of the  $N + 1$  particle system with an unperturbed ground-state described by all particles except one in the same level.

In spite of the restricted validity of the LMG model in what concerns realistic situations, the model is rich enough as to allow for important insights into open theoretical questions. The classical limit is usually defined by taking into account only the symmetric representation of the  $SU(3)$  group. Should we expect the same classical limit had we started from a different coherent state, specific of other representations? Another important point refers to the classical limit of operators which are essentially quantum in character such as parities etc. Investigations along these lines represent interesting contributions to the new born area of Dynamical Systems.

## APPENDIX A: DERIVATIVES OF THE MEAN FIELD FREE ENERGY (29)

In order to find out the minimum solutions of the mean field free energy of the model, we calculate their derivatives with respect to the variational parameters obtaining

$$\begin{aligned}
\frac{\partial \bar{F}}{\partial \theta_1} &= \cos(2\theta_1) \sin \theta_2 \sin(2\theta_3) T_3 + \sin(2\theta_1)(T_1 + \sin^2 \theta_3 T_3 - \sin^2 \theta_2(T_2 - \sin^2 \theta_3 T_3)) \\
&\quad + \chi \{ \{ \sin(2\theta_1)(T_1 - \sin^2 \theta_2 T_2) + T_3 [ \sin(2\theta_1)(1 + \sin^2 \theta_2) \sin^2 \theta_3 \\
&\quad + \cos(2\theta_1) \sin \theta_2 \sin(2\theta_3) ] \} \\
&\quad \times \{ \cos(2\theta_1)(T_1 - \sin^2 \theta_2 T_2) + T_3 [ \cos(2\theta_1)(1 + \sin^2 \theta_2) \sin^2 \theta_3 \\
&\quad - \sin(2\theta_1) \sin \theta_2 \sin(2\theta_3) ] \} \} \\
&= 0,
\end{aligned} \tag{134}$$

$$\begin{aligned}
\frac{\partial \bar{F}}{\partial \theta_2} &= 2 \sin(2\theta_2)(T_2 - \sin^2 \theta_3 T_3) + \sin(2\theta_1) \cos \theta_2 \sin(2\theta_3) \frac{T_3}{2} \\
&\quad - \sin^2 \theta_1 \sin(2\theta_2)(T_2 - \sin^2 \theta_3 T_3) + \frac{\chi}{4} \{ -\sin(2\theta_2) \sin^2(2\theta_3) T_3^2 \\
&\quad + 2 \sin(4\theta_2)(T_2 - \sin^2 \theta_3 T_3)^2 + 2 \{ \sin(2\theta_1)(T_1 - \sin^2 \theta_2 T_2) \\
&\quad + T_3 [ \sin(2\theta_1)(1 + \sin^2 \theta_2) \sin^2 \theta_3 + \cos(2\theta_1) \sin \theta_2 \sin(2\theta_3) ] \} \\
&\quad \times \{ -\sin(2\theta_1) \sin(2\theta_2) T_2 + T_3 [ \sin(2\theta_1) \sin(2\theta_2) \sin^2 \theta_3 \\
&\quad + \cos(2\theta_1) \cos \theta_2 \sin(2\theta_3) ] \} \} \\
&= 0,
\end{aligned} \tag{135}$$

$$\begin{aligned}
\frac{\partial \bar{F}}{\partial \theta_3} &= \cos(2\theta_2) \sin(2\theta_3) T_3 + \sin(2\theta_1) \sin \theta_2 \cos(2\theta_3) T_3 + \sin^2 \theta_1 \sin(2\theta_3) \\
&\quad \times T_3(1 + \sin^2 \theta_2) + \frac{\chi}{2} T_3 \{ \cos^2 \theta_2 \sin(4\theta_3) T_3 - \sin^2(2\theta_2) \sin(2\theta_3)(T_2 - \sin^2 \theta_3 T_3) \\
&\quad + \{ \sin(2\theta_1)(T_1 - \sin^2 \theta_2 T_2) + T_3 [ \sin(2\theta_1)(1 + \sin^2 \theta_2) \sin^2 \theta_3 \\
&\quad + \cos(2\theta_1) \sin \theta_2 \sin(2\theta_3) ] \} \{ \sin(2\theta_1)(1 + \sin^2 \theta_2) \sin(2\theta_3) \\
&\quad + 2 \cos(2\theta_1) \sin \theta_2 \cos(2\theta_3) \} \} \\
&= 0,
\end{aligned} \tag{136}$$

$$\begin{aligned}
\frac{\partial \bar{F}}{\partial \beta_j} &= -[\cos(2\theta_2) + \sin^2 \theta_1 \sin^2 \theta_2] A_{j2} + \sin^2 \theta_1 A_{1j} + (A_{j2} - A_{1j}) \\
&\times \left\{ \cos(2\theta_2) \sin^2 \theta_3 + \frac{1}{2} \sin(2\theta_1) \sin \theta_2 \sin(2\theta_3) + \sin^2 \theta_1 \sin^2 \theta_3 (1 + \sin^2 \theta_2) \right\} \\
&+ \frac{\chi}{2} \{ (A_{j2} - A_{1j}) \cos^2 \theta_2 \sin^2(2\theta_3) T_3 + \sin^2(2\theta_2) (T_2 - \sin^2 \theta_3 T_3) \\
&\times [A_{j2} - (A_{j2} - A_{1j}) \sin^2 \theta_3] + \{ \sin(2\theta_1) (T_1 - \sin^2 \theta_2 T_2) \\
&+ T_3 [\sin(2\theta_1) (1 + \sin^2 \theta_2) \sin^2 \theta_3 + \cos(2\theta_1) \sin \theta_2 \sin(2\theta_3)] \} \\
&\times \{ \sin(2\theta_1) (A_{1j} - A_{j2} \sin^2 \theta_2) + (A_{j2} - A_{1j}) [\sin(2\theta_{1a}) (1 + \sin^2 \theta_2) \sin^2 \theta_3 \\
&+ \cos(2\theta_1) \sin \theta_2 \sin(2\theta_3)] \} \} - \frac{1}{\beta} \left( T_j + \beta_1 A_{1j} + \beta_2 A_{j2} + \frac{\partial}{\partial \beta_j} \ln z \right) \\
&= 0, \quad j = 1, 2
\end{aligned} \tag{137}$$

where

$$A_{11} = \frac{\partial T_1}{\partial \beta_1} = -\frac{1}{z^2} (e^{-\beta_1} + 4e^{-\beta_2} + e^{(\beta_1 + \beta_2)}), \tag{138}$$

$$A_{22} = \frac{\partial T_2}{\partial \beta_2} = -\frac{1}{z^2} (e^{-\beta_2} + 4e^{-\beta_1} + e^{(\beta_1 + \beta_2)}), \tag{139}$$

$$A_{12} = A_{21} = \frac{\partial T_1}{\partial \beta_2} = \frac{\partial T_2}{\partial \beta_1} = -\frac{1}{z^2} (2e^{-\beta_1} + 2e^{-\beta_2} - e^{(\beta_1 + \beta_2)}), \tag{140}$$

$$\frac{\partial}{\partial \beta_j} \ln z = \frac{1}{z} (e^{\beta_j} - e^{-(\beta_1 + \beta_2)}), \quad j = 1, 2. \tag{141}$$

We find the solutions of this system and verify among them which correspond to minima of the free energy. These results are presented in Section IV.

## ACKNOWLEDGEMENTS

This work, which is based on part of the thesis by M. O. Terra [36], was supported by CNPq, FAPESP, and FCT (PRAXIS XXI/2/2.1/FIS/451/94). We thank C. H. Lewenkopf (UERJ) for his important contributions. We gratefully acknowledge many group discussions with A. F. R. de Toledo Piza and W. F. Wreszinski (USP).

## REFERENCES

1. V. I. Arnold, "Mathematical Methods of Classical Mechanics," Springer-Verlag, New York, 1978.
2. J. Guckenheimer and P. Holmes, "Nonlinear Oscillations, Dynamical Systems and Bifurcations of Vector Fields," Springer-Verlag, New York, 1983.
3. R. L. Devaney, "An Introduction to Chaotic Dynamical Systems," Addison-Wesley, Redwood City, 1989.
4. A. J. Lichtenberg and M. A. Leiberman, "Regular and Stochastic Motion," Springer-Verlag, New York, 1983.
5. A. M. O. de Almeida, "Hamiltonian Systems: Chaos and Quantization," Cambridge Univ. Press, Cambridge, 1990.
6. M. C. Gutzwiller, "Chaos in Classical and Quantum Mechanics," Springer-Verlag, New York, 1990.
7. F. T. Arecchi, E. Courtens, R. Gilmore, and H. Thomas, *Phys. Rev. A* **6** (1972), 2211.
8. A. M. Perelomov, *Sov. Phys. Usp.* **20** (1977), 703.
9. J. R. Klauder and B. S. Skagerstam, "Coherent States: Applications in Physics and Mathematical Physics," World Scientific, Singapore, 1985 [and references therein].
10. W.-M. Zhang, D. H. Feng, and R. Gilmore, *Rev. Mod. Phys.* **62** (1990), 867.
11. A. H. Blin, B. Hiller, M. C. Nemes, and J. da Providência, *J. Phys. A* **25** (1992), 2243.
12. A. H. Blin, B. Hiller, M. C. Nemes, and J. da Providência, *J. Phys. A* **26** (1993), 581.
13. K. Johnson, *Ann. Phys. (N.Y.)* **192** (1989), 104.
14. A. Bulgac and D. Kusnezov, *Ann. Phys. (N.Y.)* **199** (1990), 187.
15. D. Kusnezov, *Phys. Lett. B* **289** (1992), 395.
16. D. Kusnezov and J. Sloan, *Nucl. Phys. B* **409** (1993), 635.
17. D. Kusnezov, *J. Chem. Phys.* **101** (1994), 2289.
18. J. da Providência and C. Fiolhais, *Nucl. Phys. A* **435** (1985), 190.
19. J. da Providência and C. Fiolhais, *Nucl. Phys. A* **516** (1990), 53.
20. H. J. Lipkin, N. Meshkov, and A. J. Glick, *Nucl. Phys.* **62** (1965), 188.
21. S. Y. Li, A. Klein, and R. M. Dreizler, *J. Math. Phys.* **11** (1970), 975; G. Holzwarth and T. Yukawa, *Nucl. Phys. A* **219** (1974), 125; E. Moya de Guerra and F. Villars, *Nucl. Phys. A* **298** (1978), 109.
22. R. D. Williams and S. E. Koonin, *Nucl. Phys. A* **391** (1982), 72.
23. D. C. Meredith, S. E. Koonin, and M. R. Zirnbauer, *Phys. Rev. A* **37** (1988), 3499.
24. P. Leboeuf and M. Saraceno, *Phys. Rev. A* **41** (1990), 4614.
25. P. Leboeuf, "El Límite Semiclásico de Sistemas Clásicamente no Integrables," Ph.D. thesis, Universidade de Buenos Aires, Buenos Aires, 1989.
26. P. Leboeuf and M. Saraceno, *J. Phys. A* **23** (1990), 1745.
27. P. Leboeuf, D. C. Meredith, and M. Saraceno, *Ann. Phys. (N.Y.)* **208** (1991), 333.
28. A. S. Umar and A. Klein, *Nucl. Phys. A* **458** (1986), 246; A. Klein and E. R. Marshalek, *Rev. Mod. Phys.* **63** (1991), 375.
29. C. J. Thompson, "Classical Equilibrium Statistical Mechanics," Oxford Science, New York, 1988.
30. L. G. Yaffe, *Rev. Mod. Phys.* **54** (1982), 407.
31. L. G. Yaffe, *Physics Today* (1983), 50.
32. N. R. Walet and A. Klein, *Nucl. Phys. A* **510** (1990), 261.
33. A. L. Goodman, *Nucl. Phys. A* **352** (1981), 30, 45.
34. B. Lauritzen and J. W. Negele, *Phys. Rev. C* **44** (1991), 729; Y. Alhassid and B. W. Bush, *Nucl. Phys. A* **549** (1992), 43; S. Y. Tsay-Tzeng, P. J. Ellis, T. T. S. Kuo, and E. Osnes, *Nucl. Phys. A* **580** (1994), 277.
35. R. Rossignoli, A. Plastino, and H. G. Miller, *Phys. Rev. C* **43** (1991), 1599; R. Rossignoli, *Phys. Rev. C* **45** (1992), 2260.
36. M. O. Terra, "Finite Temperature Effects in the Integrable and Non-integrable Lipkin-Meshkov-Glick Model," Ph.D. thesis, Universidade de São Paulo, São Paulo, 1996.
37. M. O. Terra, A. H. Blin, B. Hiller, M. C. Nemes, C. Providência, and J. da Providência, *J. Phys. A* **27** (1994), 697.

38. C. da Providência, J. da Providência, and M. O. Terra, *J. Phys. G* **22** (1996), 351.
39. P. Ring and P. Schuck, "The Nuclear Many-Body Problem," Springer-Verlag, Berlin, 1980.
40. J. da Providência, M. Yamamura, and A. Kuriyama, *Phys. Rev. C* **50** (1994), 1720.
41. P. Kramer and M. Saraceno, "Geometry of the Time-Dependent Variational Principle in Quantum Physics," Lecture Notes in Physics, Vol. 140, p. 60, Springer-Verlag, New York, 1981.
42. V. I. Arnold, *Russian Math. Surveys* **18** (1963), 85.
43. V. I. Arnold and A. Avez, "Ergodic Problems of Classical Mechanics," Benjamin, New York, 1968.
44. C. Froeschlé, *Astron. Astrophys.* **4** (1970), 115.
45. C. Froeschlé, *Astron. Astrophys.* **5** (1970), 177.
46. G. Benettin, L. Galgani, and J. M. Strelcyn, *Phys. Rev. A* **14** (1976), 2338.